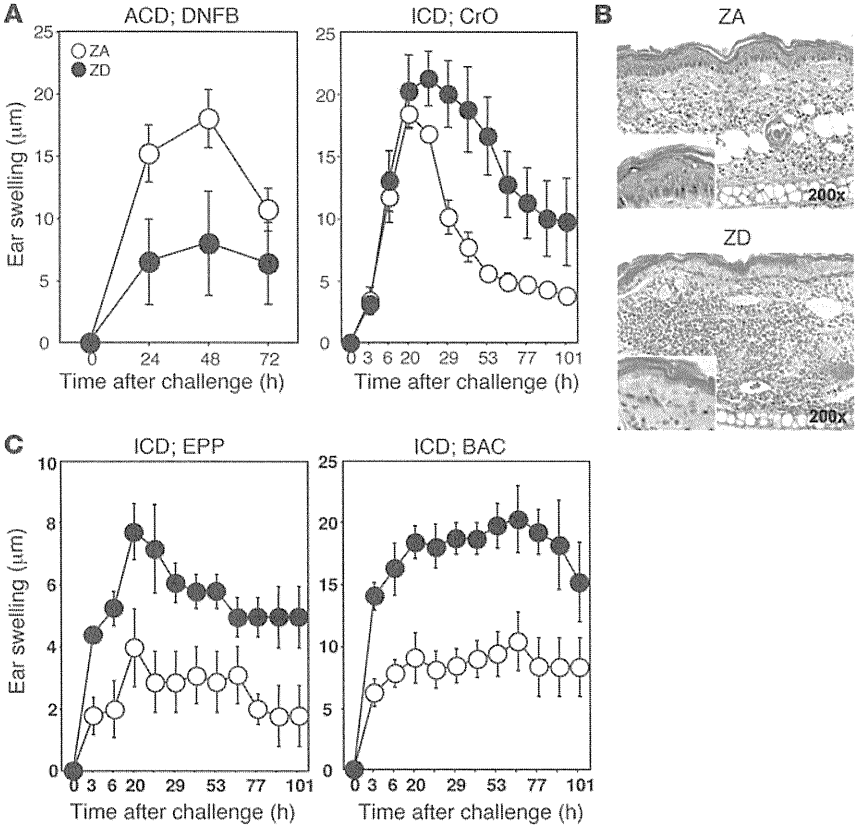

Figure 1
ZD mice demonstrate severe ICD with histological degeneration of keratinocytes. (**A** and **C**) ACD responses to DNFB and ICD responses to CrO, EPP, or BAC were induced in ZA (white circles) and ZD (black circles) mice, as described in Methods. Ear thickness was evaluated at the indicated time points. The data shown are (n = 5) the swelling responses (mean ± SD). (**B**) H&E staining of ear samples collected from ZA or ZD mice 24 hours after topical application of CrO. Original magnification: ×200; ×400 (insets). Data are representative of 3 independent experiments.

Results

Dietary Zn deficiency causes severe and prolonged irritant contact dermatitis with the histological features of AE. Symptoms of Zn deficiency in animals are similar across different species. Zn deficiency causes a well-characterized nutritional-immunological syndrome in mice (14–18, 23, 24), whereby young adults quickly manifest symptoms within 4 to 5 weeks of feeding a ZD diet containing 0.5 mg Zn/kg or more (23, 24). It is of note that, although ZD mice at approximately 70% to 80% of the control group weight exhibited visible cutaneous symptoms, such as alopecia and parakeratosis, they did not present with the characteristic inflammatory dermatitis of patients with AE (refs. 23, 24, and Supplemental Figure 1; supplemental material available online with this article; doi:10.1172/JCI58618DS1). Because AE in humans is typically seen on areas subject to repeated contact, we investigated allergic contact dermatitis (ACD) and irritant contact dermatitis (ICD) in dietary ZD mice. Five-week-old BALB/c mice were fed a ZD or Zn-adequate (ZA) diet, and at 10 weeks of age, ACD in response to dinitrofluorobenzene (DNFB) and ICD in response to croton oil (CrO) were quantified. Consistent with previous findings (24), ZD mice showed markedly decreased ear swelling responses to DNFB compared with those of ZA mice (Figure 1A). This was probably due to immunodeficiency in ZD mice, as previously reported (14, 15). Surprisingly, in contrast, the ear swelling response to CrO in ZD mice was significantly increased and prolonged compared with that of ZA mice (Figure 1A and Supplemental Figure 2). ICD caused by other skin irritant chemicals, benzalkonium chloride (BAC) and ethyl phenylpropiolate (EPP), was also tested, with similar results (Figure 1C and Supplemental Figure 2). Histological examination of ICD lesions in ZD mice revealed parakeratosis and cytoplasmic pallor, subcorneal vacuolization, and ballooning degeneration of keratinocytes and leukocyte infiltration (Figure 1B). These signs are histological features of cutaneous AE lesions in humans. No such degeneration of keratinocytes was observed in ICD lesions in ZA mice or ACD lesions in either ZA or ZD mice (Figure 1B and data not shown). These findings suggest that ICD, but not ACD, responses in ZD mice mimic the characteristic cutaneous manifestations observed in AE and can thus be considered an appropriate model for human disease.

Zn deficiency increases ATP release from keratinocytes in response to irritants. Accumulating evidence suggests that different environmental stimuli (e.g., chemical irritants) trigger adenosine 5′-triphosphate (ATP) release from keratinocytes via nonlytic mechanisms and also, more frequently, as a consequence of cell damage or acute cell death (25–27). Once released, ATP activates a family of plasma membrane receptors known as purinergic (P2) receptors. Because ATP released from chemically injured keratinocytes has been shown to cause ICD (28), we next compared the amount of ATP that was released from ZD or ZA mouse skin tissue after CrO application in ex vivo organ culture. Skin tissue obtained from ZD mice 4, 6, or 20 hours after CrO application released significantly greater amounts of ATP than tissues from ZA mice (Figure 2A). We next examined the effect of the Zn-chelating reagent TPEN on exogenous ATP release from Pam-212 keratinocytes cultured in vitro. Consistent with previous findings (26, 28), Pam-212 keratinocytes rapidly released ATP after exposure to CrO (Figure 2B). The addition of TPEN to the culture significantly augmented release of ATP in response to CrO, whereas TPEN alone failed to increase ATP release (Figure 2, B and D). The TPEN-mediated increase of ATP secretion was prevented by the addition of $ZnSO_4$ in a dose-dependent manner (Figure 2C). Furthermore, TPEN also significantly increased the secretion of ATP in response to other skin

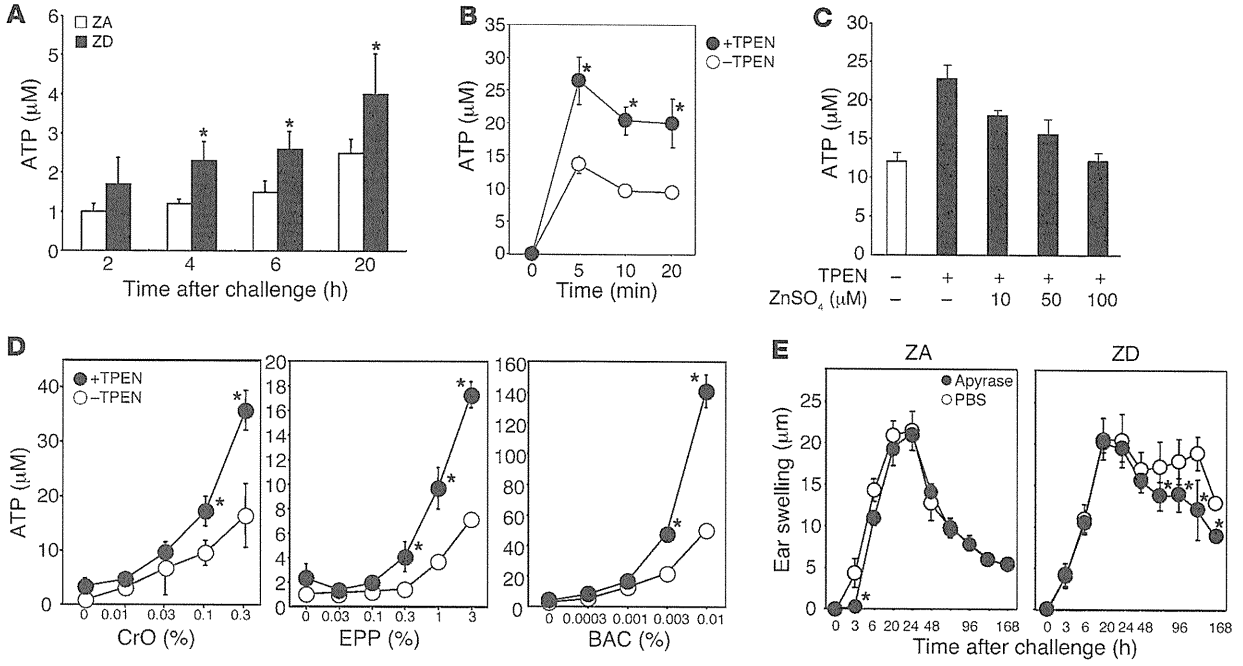

Figure 2

Zn deficiency increases ATP release by keratinocytes in response to irritant chemicals. (**A**) 1% CrO was painted on the ears of ZA (white bars) and ZD (black bars) mice ($n = 5$), and skin samples were taken at the indicated time points. ATP secretion from skin organ cultures was quantified. (**B–D**) Pam-212 keratinocytes were treated with (**B** and **C**) 0.3% CrO or (**D**) titrated concentrations of CrO, EPP, or BAC in the presence (black circles/bars) or absence (white circles/bars) of 2 μM TPEN. ATP in the culture supernatants was quantified at (**B**) the indicated time points or (**C** and **D**) 10 minutes after stimulation. (**C**) Cells were cultured with 10–100 μM $ZnSO_4$. *$P < 0.05$, compared with cells that were not treated with TPEN. (**E**) ICD responses to CrO were induced, as described in Figure 1. ZA and ZD mice ($n = 5$) received local injections of potato apyrase on the right ear (black circles) or PBS alone on the left ear (white circles) before and after CrO application to both ears. The data shown are the swelling responses (mean ± SD). *$P < 0.05$, between the apyrase and PBS treatments. Data are representative of 3 independent experiments.

irritant chemicals (herein, EPP and BAC) (Figure 2D). Together, these findings clearly indicate that Zn deficiency and irritant chemicals synergistically increase ATP release from keratinocytes.

Although various types of cells release ATP, the mechanism underlying the release of ATP is controversial (29). Several studies have shown that the release of ATP is reduced by carbenoxolone (CBX), suggesting the involvement of connexin or pannexin membrane channels in the release. In addition, inhibition of ATP release by vesicular ATPase inhibitors or intracellular Ca^{2+} deprivation was also reported, suggesting that the mechanisms of ATP release could include exocytosis. As shown in Supplemental Figure 3, CBX significantly decreased ATP release from CrO-treated keratinocytes, and, more importantly, it dramatically inhibited TPEN-mediated increase of ATP secretion. By contrast, BAPTA-AM, a membrane-permeable, strong Ca^{2+}-chelator, did not affect the CrO-evoked ATP release from keratinocytes. These results clearly indicate that membrane channel–mediated diffusible mechanisms, but not Ca^{2+}-dependent exocytosis, play a key role in the release of ATP from keratinocytes treated with CrO.

Previous studies have shown that hydrolysis of nucleotides by s.c. injections of soluble ecto-nucleoside triphosphate diphosphohydrolase (NTPDase; soluble potato apyrase) diminishes early inflammation in ICD (28). As shown in Figure 2E, we obtained similar results in ZA mice. In contrast, injections of apyrase before and after CrO application in ZD mice significantly decreased the late ICD response (Figure 2E). This suggests that aberrant ATP release from epidermal keratinocytes in response to irritant chemicals contributes, at least in part, to the prolonged ICD response in ZD mice.

Aberrant chemokine gene expression in ZD keratinocytes. In general, there are very few differences in the histological, immunohistochemical, and electron microscopy findings in ACD and ICD (30). However, ICD is thought to be mediated via T cell–independent innate immunity, because the ear swelling response to CrO is similar for both athymic and normal mice and neutrophils are the predominant cells in ICD (31). Recent work has shown that different patterns of inflammatory chemokines may distinguish between ACD and ICD (32). To explore such mechanisms for increased ICD in Zn deficiency, we first analyzed gene expression profiles for 44 chemokines in epidermal sheets obtained from ZA and ZD mice 24 hours after vehicle or CrO exposure. Profound differences in chemokine gene expression were observed (Supplemental Figure 4). However, *Cxcl1* was markedly induced by CrO in both ZA and ZD mice, suggesting a possible association between this chemokine and neutrophil recruitment. Because CXCL1 and CXCL2 are known to mediate neutrophil influx into tissues (33), we next quantified their mRNA expression in epidermal sheets obtained from ZA and ZD mice after vehicle or CrO application in vivo. Quantitative real-time PCR demonstrated that Zn deficiency resulted in a significant increase of *Cxcl1* mRNA 4 and 24 hours after CrO exposure and *Cxcl2* mRNA at 4 hours (Figure 3, A and B). The same enhancing effects of Zn deficiency for the chemokine mRNA expression were observed when mice were treated with BAC (Supplemental Figure 5A). In addition, in vitro exposure of Pam-

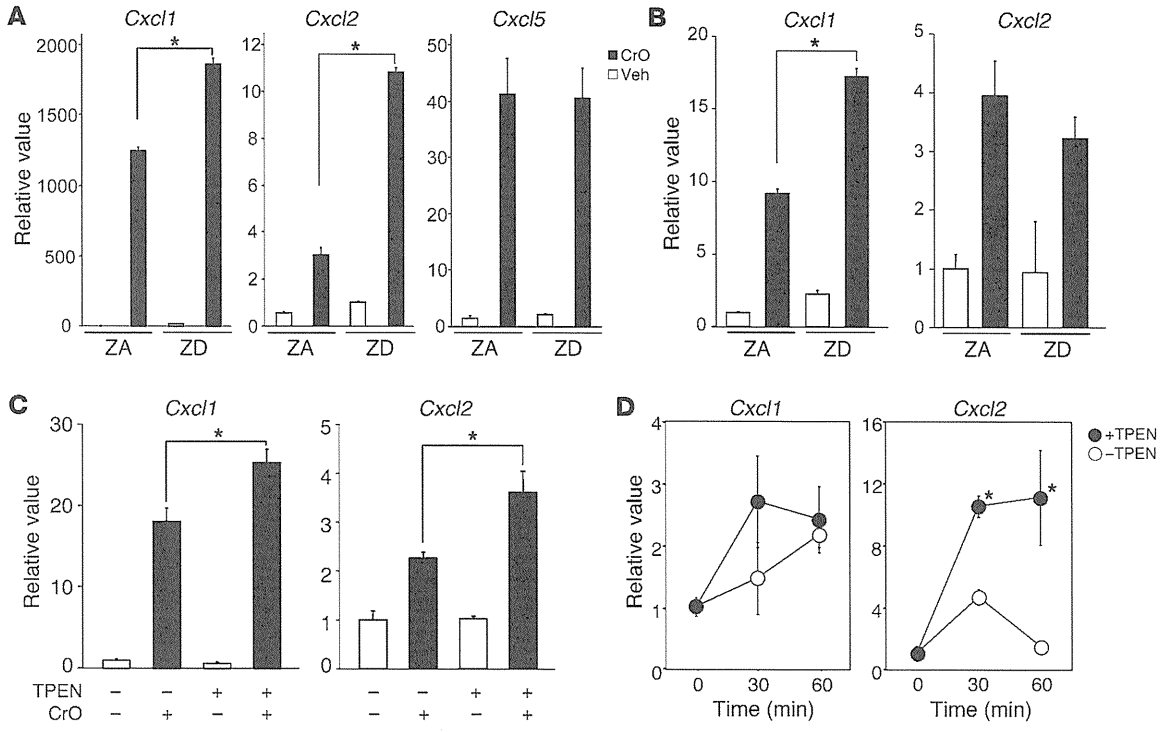

Figure 3

Zn deficiency increases *Cxcl1* and *Cxcl2* gene expression in keratinocytes after treatment with CrO. (**A** and **B**) 1% CrO (black bars) or vehicle alone (white bars) was painted on the ears of ZA and ZD mice (n = 5). Epithelial sheets were obtained from the ears at (**A**) 4 hours or (**B**) 24 hours, and total RNA was extracted. (**C**) Pam-212 keratinocytes were cultured in the presence or absence of 2 μM TPEN. Total RNA was extracted 4 hours after 0.3% CrO (black bars) or vehicle (white bars) exposure. (**D**) Pam-212 keratinocytes were treated with 100 μM ATPγS in the presence (black circles) or absence (white circles) of 2 μM TPEN. Total RNA was extracted 4 hours after ATPγS exposure. Quantitative real-time RT-PCR analysis of *Cxcl1* and *Cxcl2* was performed. *Cxcl5* was examined as control in **A**. mRNA expression was normalized to *Gapdh*. The fold induction (mean ± SD) was calculated from the normalized mRNA expression by CrO- or ATP-stimulated keratinocytes relative to nonstimulated ZA keratinocytes. *P < 0.05, compared with cells that were from ZA mice or not treated with TPEN. Data are representative of 3 independent experiments.

212 keratinocytes to CrO rapidly induced *Cxcl1* and *Cxcl2* mRNA (Figure 3C). When TPEN was added to the cultures, significant further augmentation of CrO-induced chemokine mRNA accumulation was observed, which was not seen with TPEN alone (Figure 3C). Similar results were obtained in BAC-treated keratinocytes (Supplemental Figure 5B). Furthermore, consistent with recent findings (34), exogenous ATPγS induced *Cxcl1* and *Cxcl2* mRNA expression by ZA Pam-212 keratinocytes (Figure 3D). Together, our results suggest that Zn deficiency indirectly augments *Cxcl1* and *Cxcl2* gene expression in CrO-stimulated keratinocytes via increased ATP release, as observed in Figure 2. Interestingly, Zn deficiency further augmented ATPγS-induced *Cxcl2*, but not *Cxcl1*, mRNA expression (Figure 3D).

Loss of epidermal Langerhans cells in Zn deficiency. Langerhans cells (LCs) are a long-lived subset of tissue DCs that reside in the epidermis. LCs acquire skin antigens and then migrate to skin-draining LNs in both inflammatory and steady-state conditions (35). Recently, it has been shown that CD39, which is expressed exclusively by LCs in the epidermal compartment, is responsible for ecto-NTPDase activity in LCs (28). Because the P2-receptor signaling pathway is negatively regulated by NTPDase-dependent hydrolysis of ATP, LC-associated CD39 plays a protective role against ATP-mediated inflammatory signals by hydrolyzing extracellular nucleotides released by keratinocytes in ICD responses (28). Therefore, we next examined the number, distribution, and morphology of epidermal LCs in Zn deficiency. Although epidermal cells prepared from the ear skin of ZA mice contained a normal contingent of LCs (I-A^{d+} $CD11c^+$ cells), in mice fed the ZD diet, the number of epidermal LCs decreased with time on the diet, and few LCs were observed after 6 weeks (Figure 4, A and B). Immunofluorescence microscopy confirmed the loss of LCs from epidermal sheets prepared from mice fed a ZD diet for 6 weeks (Figure 4C). In contrast, the frequency and morphology of dendritic epidermal T cells (DETCs; $Thy\text{-}1^+$ cells), which are skin-resident γδ T cells expressing a monoclonal T cell receptor containing Vγ3 and Vδ1 determinants, in ZD mice was normal even after 6 weeks (Figure 4, C and D). It is of note that the proportions of I-A^+ $CD11c^+$ cells in axillary and inguinal lymph nodes, including migratory DCs (e.g., LCs) and resident lymphoid DCs, from ZD mice were comparable in number to those of ZA mice (Figure 4A). The possibility that Zn deficiency downregulates the expression of cell surface markers on epidermal LCs was considered unlikely, because treatment of epidermal sheets with TPEN (2 μM) for 4 days failed to decrease surface expression of I-A^d and CD11c on murine epidermal LCs (data not shown).

Loss of epidermal LCs in patients with AE. We next examined the number, distribution, and morphology of epidermal LCs in human skin

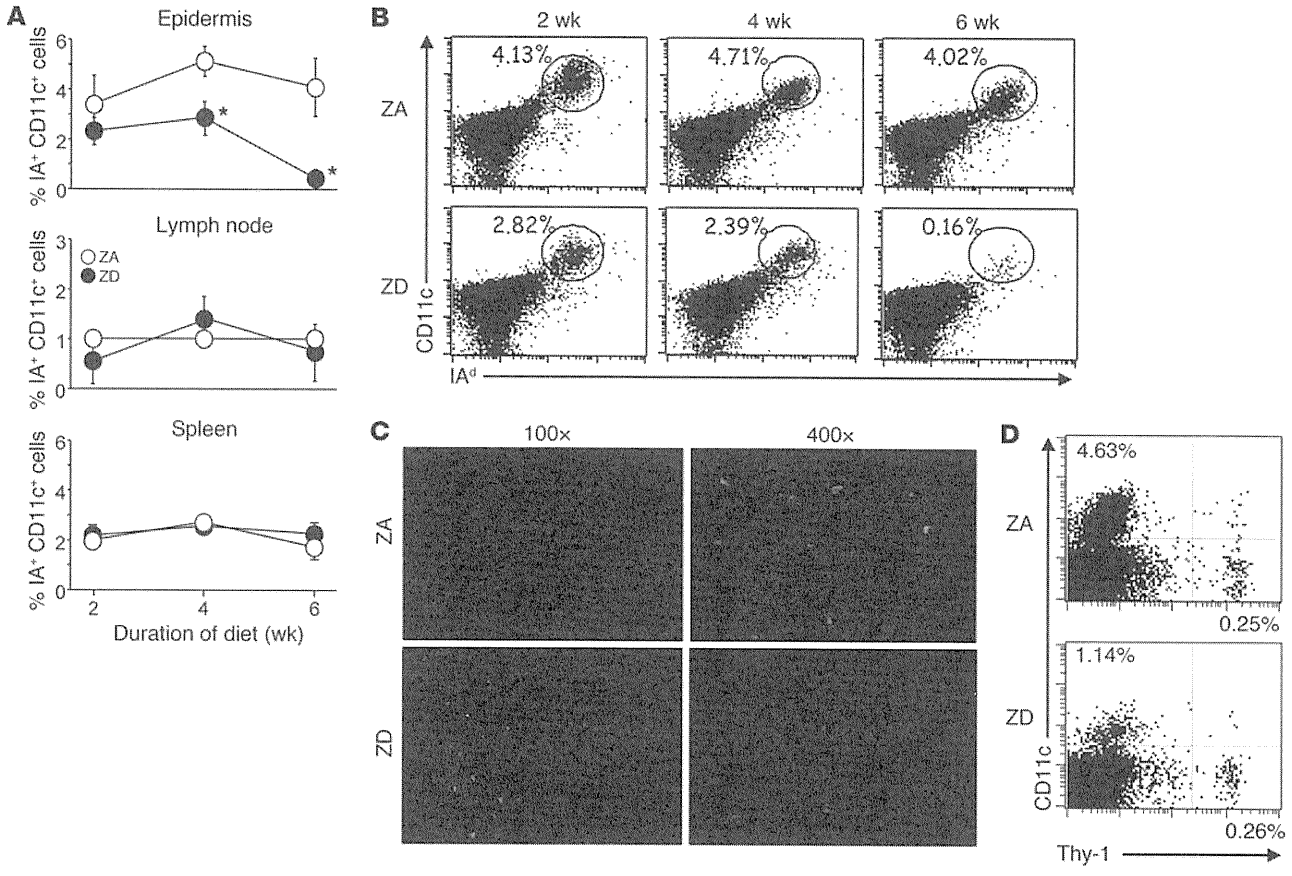

Figure 4

Loss of epidermal LCs in Zn deficiency. (**A**) Cell suspensions of epidermis, axillary, and inguinal lymph nodes and spleens were prepared from mice fed ZA (white circles) or ZD (black circles) diets for the indicated time and stained for I-A and CD11c antigens. The percentages of I-A and CD11c double-positive cells were assessed within each live-gated cell population. Results are the mean ± SD (n = 3). *P < 0.05, compared with mice fed the ZA diet. A representative FACS analysis of live-gated epidermal cell suspensions from mice fed ZA or ZD diets for 6 weeks and stained for (**B**) I-A and CD11c or (**D**) Thy-1 and CD11c antigens. Numbers indicate the percentages of cells in the (**B**) circles or (**D**) gate. (**C**) Immunofluorescence of epidermal whole mounts stained for I-A (red) and Thy-1 (green) from mice fed ZA or ZD diets for 6 weeks. Original magnification, ×100 (left panels); ×400 (right panels). Data are representative of 3 independent experiments.

samples obtained from inflammatory lesions of patients, including those with atopic dermatitis, psoriasis vulgaris, and hereditary and acquired AE, by immunofluorescence staining analyses. Langerin$^+$ LCs were found to be regularly scattered throughout the epidermis of control specimens but were absent from the epidermis of patients with AE (Figure 5A). HLA-DR antigens were also rarely expressed in the epidermis of AE specimens but were present on the surface of dermal mononuclear cells in the same specimens (Figure 5B). Interestingly, skin biopsy specimens obtained from the same lesions in a patient with hereditary AE after 6 months of oral Zn supplementation revealed recolonization of the epidermis with LCs, accompanied by marked clinical improvement (Figure 5C). We also examined immunohistochemical staining with formalin-fixed skin samples obtained from patients with AE. As shown in Supplemental Figure 6A, langerin$^+$ LCs were absent from the epidermis of the patients with AE. Quantitation of langerin$^+$ cells in the epidermis (n = 3) revealed that the number of LCs in the lesional epidermis of AE specimens was significantly decreased as compared with that in normal skin (the mean positive cell per field ± SD was 16.7 ± 2.8 in normal skin and 0.4 ± 0.3 in AE skin; P < 0.05). Similarly, the number of HLA-DR$^+$ cells in the lesional epidermis of AE specimens was also significantly decreased (the mean positive cell per field ± SD was 10.4 ± 0.6 in normal skin and 3.7 ± 2.7 in AE skin; P < 0.05). Taken together with the findings in ZD mice (Figure 4), these findings indicate that Zn deficiency results in depletion of epidermal LCs.

Decreased steady-state production of TGF-β1 in cutaneous, but not mucosal, epidermis in Zn deficiency. Although the mechanisms that regulate LC homeostasis in the steady state are yet to be fully elucidated, previous studies demonstrated that LC development requires TGF-β1 (35). Mice lacking TGF-β1 possess no LCs, owing to either a failure in LC differentiation, survival, or both (35, 36). Therefore, we next assessed the cutaneous expression of TGF-β1 in Zn deficiency. Mucosal TGF-β1 levels in the large and small intestine in ZD mice were comparable to those in ZA mice (Figure 6B), whereas the skin tissue obtained from ZD mice contained significantly lower amounts of TGF-β1 than that from ZA mice (Figure 6A). To detect the TGF-β activity in the skin samples, MFB-F11 reporter cells were used in a bioassay (Figure 6C and ref. 37). Secreted alkaline phosphatase (SEAP) activity was not detected without activation of the samples by HCl, suggesting that murine skin contains TGF-β protein in a latent form. However, after activation, skin samples

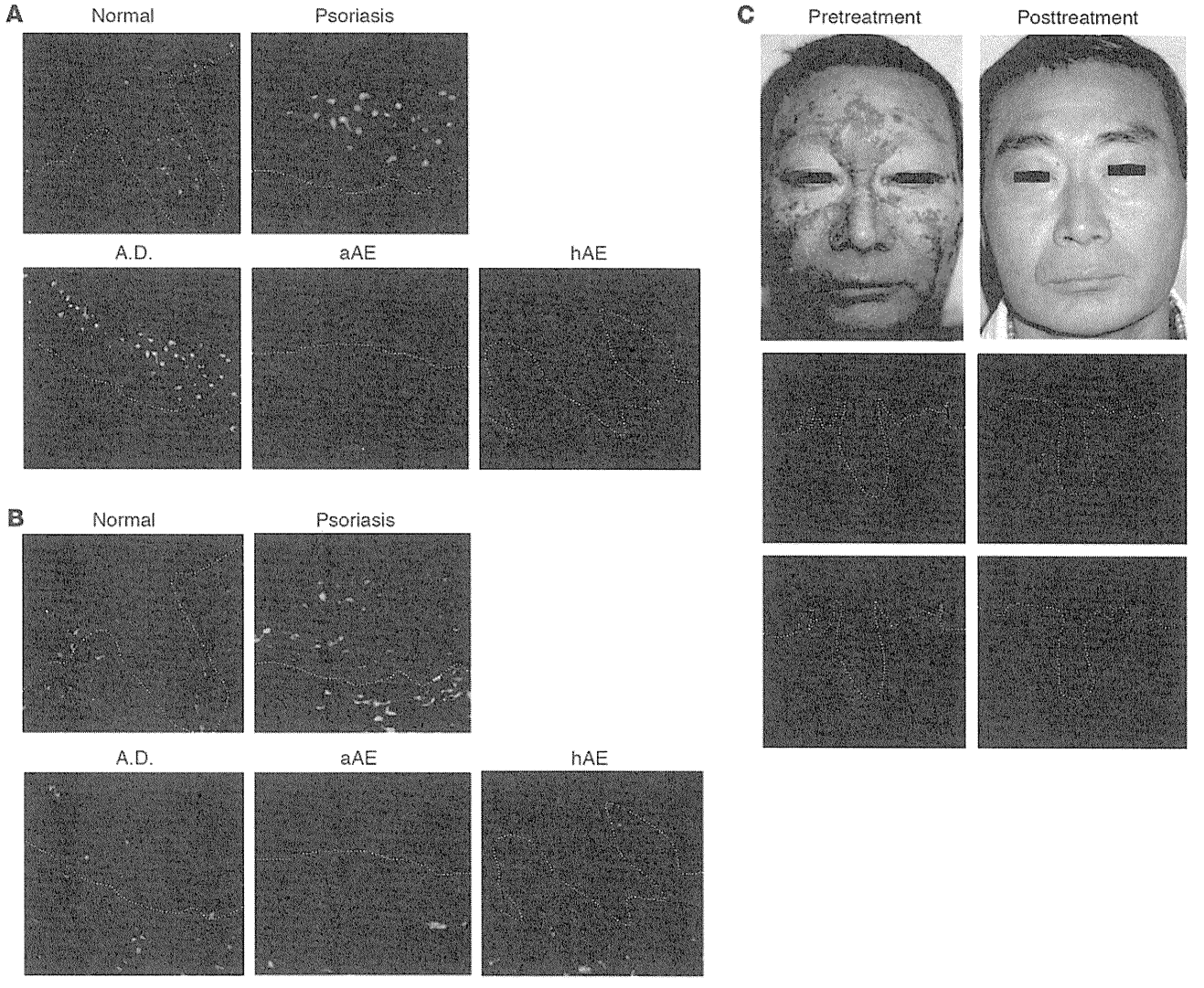

Figure 5

Loss of epidermal LCs in patients with AE. (**A** and **B**) Immunohistochemical staining for HLA-DR (green) and langerin (red) in the erythematous lesions of patients with psoriasis vulgaris (psoriasis), atopic dermatitis (A.D.), hereditary AE (hAE), and acquired AE (aAE) or normal skin. Original magnification, ×200. (**C**) Clinical appearance and immunohistochemical staining of a patient with hereditary AE before and after treatment by oral Zn supplement. White dotted lines denote the epidermis/dermis interface. Original magnification, ×200.

obtained from ZD mice were found to mediate significantly less SEAP activity than those from ZA mice (Figure 6C). In addition, we found that *Tgfb1* mRNA levels in epidermal sheets from ZD mice were significantly lower than those from ZA mice (Figure 6D). These results suggest that Zn deficiency decreases epidermal TGF-β1 expression in the steady state, and this might, at least in part, be associated with the reduction of epidermal LCs in Zn deficiency.

Because recent studies have shown that TGF-β1 has antiapoptosis effects in LCs or DCs (38, 39), we next assessed for apoptosis in epidermal LCs freshly isolated from ZA and ZD mice. As shown in Supplemental Figure 7A, the incidence of annexin V^+ cells in LCs from mice fed ZD diets for 3 weeks was slightly, but significantly, higher than that from mice fed ZA diets. We next performed in vitro experiments to obtain additional evidence for the hypothesis that Zn deficiency directly induces apoptosis of LCs. After in vitro culture of epidermal cell suspensions obtained from ZA mice with varying concentrations of TPEN for 48 hours, 5 μM TPEN significantly increased the incidence of annexin V^+ LCs (Supplemental Figure 7B). Similarly, we also found a significant increase of apoptosis in human monocyte-derived LCs cultured with TPEN at a concentration of 5 μM (Supplemental Figure 7C). Notably, consistent with a previous finding in HaCaT keratinocytes (40), Pam-212 keratinocytes cultured with 5 μM TPEN for 48 hours demonstrated no changes in cell viability and growth (data not shown). These results suggest that, in addition to the reduced TGF-β1 in epidermis, severe Zn deficiency may directly induce apoptosis in LCs, resulting in the loss of LC networks in ZD mice.

Enhanced ICD in the absence of LCs. At present, there are 2 types of LC ablation murine models. The first LC ablation model uses transgenic langerin$^-$ diphtheria toxin A (DTA) mice (41), which constitutively lack LCs. The second uses mice that express EGFP fused with a diphtheria toxin receptor (DTR) under the control

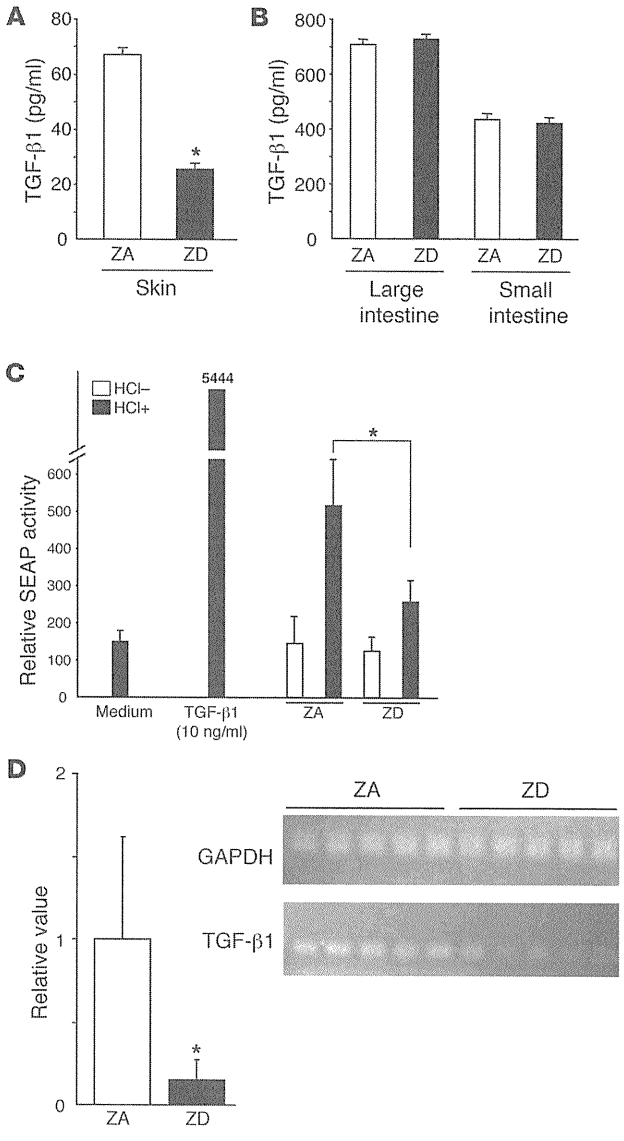

Figure 6
Decreased TGF-β1 production in the skin of ZD mice. (**A** and **B**) Samples of (**A**) skin tissue or (**B**) mucosal tissue were taken from the backs of mice fed a ZA (white bars) or ZD (black bars) diet for 5 weeks and cultured for 24 hours (n = 5). TGF-β1 secretion in the ex vivo skin or mucosa organ cultures was assessed by ELISA assays. (**C**) SEAP activity of the skin samples measured using MFB-F11 cells with or without HCl in the culture system. (**D**) Quantitative real-time RT-PCR for the detection of *Tgfb1* and *Gapdh* mRNAs in epidermis from the ears of mice fed a ZA (white bar) or ZD (black bar) diet for 5 weeks. The fold induction was calculated from normalized mRNA expression by the epidermis of ZD mice relative to that of ZA mice. Results are the mean ± SD (n = 5). $^*P < 0.05$, compared with mice fed the ZA diet. Data are representative of several experiments with similar results.

of the langerin promoter, which are known as langerin-EGFP-DTR mice (42) and langerin-DTR mice (43). After i.p. injection of diphtheria toxin (DT) into langerin-EGFP-DTR mice, LCs do not repopulate for at least 4 weeks, while the number of langerin$^+$ dermal DCs in the skin recover to the basal level about 7 days after depletion by DT (44). Langerin-EGFP-DTR mice 14 days after treatment with DT are used as a model to deplete LCs alone. Fourteen days after treatment with DT, langerin-DTR mice and C57BL/6 (B6) mice were treated with 5%, 1%, and 0.5% CrO on the ears and monitored for ear swelling. As expected, the ear swelling response to 1% and 0.5% CrO in langerin-DTR mice was significantly increased at 12 and 24 hours after application compared with that in corresponding B6 mice (Figure 7). These results suggest that depletion of LCs enhances ICD responses, consistent with our findings that ZD mice lacking epidermal LCs exhibited increased ICD responses to 1% CrO (Figures 1 and 4).

Discussion

Although the skin is commonly involved and is often one of the first organs affected in Zn deficiency, the underlying pathophysiology of the inflammatory skin manifestation in AE remains unclear. Nearly pathognomonic in the histopathologic examination of AE is the presence of "necrolysis," a term describing cytoplasmic pallor, vacuolization, ballooning degeneration, and subsequent confluent necrosis of keratinocytes within the epidermis (8). As several in vitro studies have shown that Zn deficiency can induce cell death in HaCaT keratinocytes via apoptosis or necrosis (40, 45, 46), one of the mechanisms of epithelial damage observed in AE lesions might be by increased death of keratinocytes. However, the characteristic inflammatory dermatitis in clinical AE is seen only in the acral areas, suggesting the participation of additional cellular processes, which could account for the restricted localization of the dermatitis and the severe cutaneous inflammation in immunodeficient AE patients.

Our data, which we believe to be novel, reveal that irritants, but not haptens, can cause severe skin inflammation in immunodeficient ZD mice, providing a biologic basis for understanding the pathogenesis of AE. We found that ICD responses in ZD mice exhibited similar histological features similar to those of the characteristic dermatitis in clinical AE, highlighting the possibility that the acral, periorificial, and anogenital dermatitis in AE might be caused by contact with different irritants in daily life, such as chemicals, foods, urine, and feces, etc. We have addressed the mechanisms responsible for the severe and prolonged ICD in ZD mice and have identified several abnormalities which we believe to be novel, including aberrant chemokine gene expression and ATP release by keratinocytes in response to irritant chemicals. These 2 abnormalities are closely associated, because extracellular ATP induces keratinocyte *Cxcl1* and *Cxcl2* gene expression, major chemoattractants for neutrophils (Figure 3D and refs. 33, 34). Together with the insight that neutrophils are the pathogenic cells in ICD (31), our results suggest that ATP plays a key role in the pathogenesis of severe and prolonged ICD in Zn deficiency. This notion is supported by the finding that local injection of apyrase significantly diminished the ICD response in ZD mice (Figure 2E). Our in vitro assay revealed that membrane channel–mediated diffusible mechanisms play a pivotal role in the Zn deficiency–induced increased ATP release from irritant-stimulated keratinocytes (Supplemental Figure 3). However, because chemical irritants also trigger ATP release from keratinocytes as a consequence of cell damage or acute cell death (26, 28), Zn deficiency and irritants may synergistically induce keratinocyte cell damage, as shown in Figure 1B, leading to increased ATP release in vivo.

We found that ex vivo ATP release from CrO-treated skin was increased in Zn deficiency (Figure 2A). This observation is in line

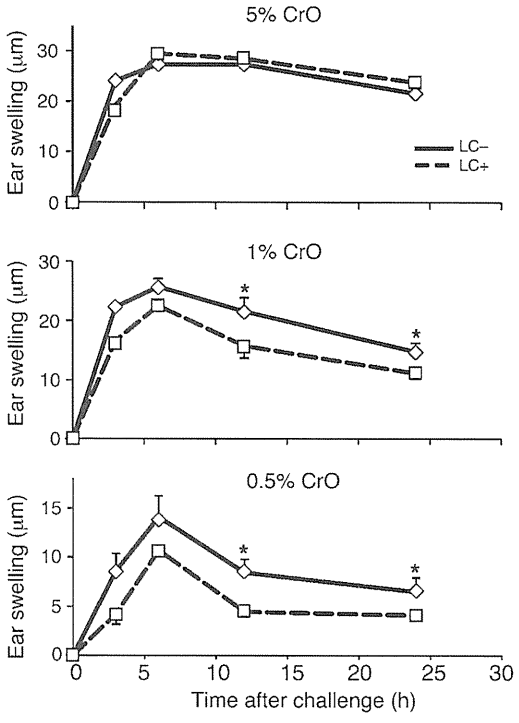

Figure 7
Enhanced ICD in the absence of LCs. Fourteen days after treatment with DT, langerin-DTR (LC–) and B6 (LC+) mice were applied with 5% (mean ± standard error [SE]; n = 4 and 6, respectively), 1% (mean ± SE; n =10 and 16, respectively), and 0.5% (mean ± SE; n = 6 and 10, respectively) CrO on the ears and monitored for ear swelling 3, 6, 12, and 24 hours later. Data are presented as the mean ± SEM (μm) and are a representative of 3 independent experiments. *P < 0.05, between langerin-DTR and corresponding B6 mice.

with our in vitro findings that Zn deficiency augments the release of ATP from irritant-stimulated Pam-212 keratinocytes. In addition, the decreased number of epidermal LCs observed in ZD mice (Figure 4) might also contribute to the increased ATP release from skin organ cultures ex vivo (Figure 2A) as well as the severe and prolonged ICD responses in vivo (Figure 1). Mechanisms include loss of the potent ecto-NTPDase activity of LC-associated CD39, which plays a protective role against ATP-mediated inflammation in ICD responses (28). Taken together, our results suggest that the inflammatory skin manifestations in patients with AE may occur as a result of excessive ICD responses, presumably due to aberrant ATP release upon repeated exposure to various irritants in daily life.

According to our data, Zn deficiency decreases epidermal TGF-β1 expression and its activity in the steady state. While the signaling via TGF-β receptor has been well defined, the homeostatic regulation of TGF-β is largely obscure. So far, the best-characterized regulator (inducer) of TGF-β expression is TGF-β itself (47), and an autocrine production of TGF-β1 is generally required for the homeostasis of various cell types, including LCs (48). Therefore, signaling molecules downstream of TGF-β receptor, such as Smad proteins, are thought to be involved in the regulation of their TGF-β production. Since a number of Zn finger transcription factors (e.g., ZNF580) has been reported to be associated with TGF-β signaling (49), Zn deficiency might decrease the autocrine production of TGF-β1 in LCs and keratinocytes by multiple pathways via those transcription factors.

The present results indicate that Zn deficiency induced the loss of epidermal LCs. Since several lines of evidence have indicated that TGF-β1 governs LC homeostasis (36, 50), the reduced TGF-β1 in epidermis may be, at least in part, responsible for the LC disappearance. The other possible mechanism for LC depletion is apoptosis, because several studies have suggested that Zn is an important physiological regulator of apoptosis (51). Indeed, the incidence of apoptosis in epidermal LCs in ZD mice was increased in the steady state (Supplemental Figure 7A). We also found that murine and human LCs underwent apoptosis when cultured with TPEN at a concentration of 5 μM (Supplemental Figure 7, B and C), while the culture condition did not induce apoptosis in keratinocytes (data not shown), suggesting that LCs are more sensitive to Zn deficiency-induced apoptosis. Taken together with the findings that TGF-β1 has antiapoptosis effects (38, 39), our results suggest that severe Zn deficiency may induce apoptosis in LCs through synergy between its direct effect and the reduced TGF-β1 expression, resulting in the loss of LC networks. Additional studies are needed to determine the impact of TGF-β1 on LC survival in vivo and the paramount mechanism underlying LC disappearance in ZD mice and patients with AE.

A previous study has reported that, in transgenic langerin-DTA mice, depletion of LCs does not affect ICD responses induced by 0.5%–2.5% sodium dodecyl sulfate or 5% BAC (41). In our study using langerin-EGFP-DTR mice, however, the ear swelling response to 1% and 0.5% CrO was significantly increased (Figure 7), consistent with the previous findings that LC-associated CD39 plays a protective role against ATP-mediated inflammation in ICD (28). Nevertheless, both langerin-DTR mice and control mice developed a similar degree of ear swelling after application of 5% CrO (Figure 7), as previously observed in transgenic langerin-DTA mice (41). Since CrO induces ATP release from keratinocytes in a dose-dependent manner (Figure 2), it is possible that an excess ATP release in ICD in response to a high dose of CrO in vivo might be beyond the capacity of NTPDase-dependent hydrolysis by LCs. Alternatively, differences in irritants or depletion timing might explain the phenotypic differences among the LC ablation models (41, 42). Further detailed analysis under different conditions is needed to reveal the functions and significance of LCs in ICD.

Methods

Animals and diet. Five-week-old female BALB/c mice were purchased from Oriental Yeast Co. Ltd. Mice were maintained under specific pathogen-free conditions throughout this study. ZD diet was purchased from CLEA Japan Inc. The mice were fed a powdered ZD diet or control diet from 5 to 11 weeks of age (n = 5–10 per group). Both diets were of almost the same nutritional quality, differing only in terms of Zn content (Zn, 0.11–0.38 mg/100 g in ZD diet, 6.00 mg/100 g in control diet). Langerin-EGFP-DTR mice on a B6 background (provided by Bernard Malissen, Université de la Méditerranée, Aix-en-Provence, Gap and Marseille, France) express a high-affinity human DTR in the langerin locus, as described previously (44). After i.p. injection of 1,000 ng DT in PBS, LCs do not repopulate for at least 4 weeks, while the number of langerin$^+$ dermal DCs in the skin recovers to the basal level about 7 days after depletion by DT (44).

Patients. Biopsies were obtained from lesional skin of patients, including those with atopic dermatitis, psoriasis vulgaris, hereditary AE (pretreatment and posttreatment with oral Zn sulfate), and acquired AE. Addition-

ally, control biopsies were obtained from healthy volunteers. The samples were snap frozen in liquid nitrogen and stored at –80°C.

Reagents and antibodies. DNFB, CrO, BAC, EPP, TPEN, CBX, and BAPTA-AM were purchased from Sigma-Aldrich. $ZnSO_4$ was purchased from Kanto Chemical Inc. FITC-conjugated anti-human HLA-DR, anti-mouse I-A^d, and CD90 (Thy-1) mAbs and PE-conjugated anti-mouse CD11c and I-A^d mAbs were purchased from BD Biosciences. Purified and PE-conjugated anti-human langerin mAbs were purchased from Abcam and R&D Systems, respectively.

ACD and ICD responses. For the induction of chemically induced allergic skin inflammation, mice were topically treated with 20 μl 0.5% DNFB dissolved in acetone/olive oil (4:1), which was painted onto the shaved abdomen at days 0 and 1. The ears were then challenged with 10 μl of 0.2% DNFB on the right ear and vehicle alone on the left ear on day 5. For chemically induced irritant skin inflammation, mice received topical application of 1% CrO, 10% BAC, or 30% EPP on the right ear and vehicle alone on the left ear. Swelling responses were quantified (right ear thickness minus left ear thickness) by a third experimenter using a micrometer, as described previously (28). In some experiments, potato apyrase grade VII (0.2 U/ear; Sigma-Aldrich) was injected s.c. into the ear 10 minutes before and 1 hour after CrO painting (28). In experiments with langerin-EGFP-DTR mice, 5%, 1% and 0.5% CrO was painted on the ears.

Quantification of ATP release from the skin and keratinocytes. ATP secretion from skin organ culture was quantified, as previously reported (52). Skin samples were taken from both ears immediately. s.c. fat was removed with a scalpel, and the skin explants were prepared by being cut into 8.0-mm circular pieces. The 2 pieces of skin from the 2 ears were floated with the epidermis side upward in 12-well plates containing 4 ml PBS and incubated on ice for 10 minutes. In some experiments, Pam-212 keratinocytes cultured in DMEM medium containing 10% FCS, 10 mM HEPES, 0.25 μg/ml gentamicin, and 2 mM L-glutamine were pretreated with 2 μM TPEN for 6 hours and then cultured with PBS with CrO, BAC, or EPP. ATP concentrations in the supernatants were then quantified using the luciferin-luciferase assay.

Preparation of epidermal cell suspensions and epidermal sheets. The ears were removed, mechanically divided into dorsal and ventral cutaneous sheets, and then incubated with a 0.5% solution of trypsin (type XI, Sigma-Aldrich) in PBS for 30 minutes at 37°C to separate the epidermis from the underlying dermis. After removal of the loosened dermis, the epidermal sheets were gently agitated with 0.05% DNase (DN25; Sigma-Aldrich) in PBS for 10 minutes, and the resulting EC suspension was passed through a nylon mesh to remove hair and stratum corneum prior to use. The viability determined by trypan blue exclusion was always more than 90% (53). For immunohistological staining, epidermal sheets were prepared from ear skin by incubation in 0.5 M ammonium thiocyanate (37°C for 20 minutes), fixed in acetone (–20°C for 30 minutes), and rehydrated in PBS (36).

Preparation of monocyte-derived LCs. Monocyte-derived LCs were cultured from PBMCs, as described previously (54). Briefly, monocytes were isolated by depletion of magnetically labeled nonmonocytes (Monocyte Isolation Kit II; Miltenyi Biotec) from plastic-adherent PBMCs obtained from healthy blood donors. Monocytes were cultured with 1,000 U/ml recombinant human GM-CSF (R&D Systems), 1,000 U/ml recombinant human IL-4 (R&D Systems), and 10 ng/ml human platelet-derived TGF-β1 (R&D Systems) for 7 days.

Flow cytometry. Single-cell suspensions (5×10^5) of epidermal sheets, inguinal and axillary lymph nodes, and spleens obtained from ZA and ZD mice (5 mice per group) were stained for LCs with FITC-conjugated anti–I-A^d and PE-conjugated anti-CD11c mAbs or for DETCs with FITC-conjugated anti–Thy-1 mAb for 30 minutes at 4°C. Live/dead discrimination was performed using propidium iodide (Sigma-Aldrich). After washing, samples were analyzed on a FACSCalibur (BD Biosciences). Annexin V–FITC and propidium iodide staining was carried out according to the instructions of BD Pharmingen.

Histological examination. Tissue specimens from the ears from ZA or ZD mice were surgically removed immediately after determination of ear swelling, embedded in OCT compound (Tissue-tek), frozen in liquid nitrogen, and stored at –80°C until use. Cryostat sections were fixed in absolute acetone and stained with H&E. For immunohistochemical staining, murine epidermal sheets were stained for LCs and DETCs with PE-conjugated anti–I-A^d mAb or FITC-conjugated anti–Thy-1 mAb, washed, and analyzed by fluorescence microscopy. For human skin samples, cryostat sections were double stained with FITC-conjugated anti-HLA-DR and PE-conjugated anti-langerin mAbs, washed, and analyzed by fluorescence microscopy. For formalin-fixed skin samples, they were stained with anti–HLA-DR and anti-langerin mAbs, incubated with biotinylated goat anti-mouse immunoglobulins, and then incubated with streptavidin-peroxidase. Reactions were developed with aminoethylcarbazole. Sections were incubated with a DAKO LSAB Kit, HRP (DakoCytomation) and then counterstained with Mayer's hematoxylin. Positive (HLA-DR and langerin) cells were counted at high magnification (×400) in 4 different fields, and the average number of positive cells per field was calculated for each sample.

DNA microarray analysis. RNA was harvested using TRIzol (Invitrogen) from epidermal sheets obtained from ZA and ZD mice 24 hours after vehicle or CrO exposure. Preparation of cRNA and hybridization of probe arrays (U133.2.plus) was performed according to the manufacturer's instructions (Affymetrix). Data were analyzed according to the MIAME rule. The average μ and SD σ values of ZA and ZD mouse distributions are (–0.049, 1.35) and (–0.041, 1.34), respectively. The accession numbers for each chemokine gene are as follows (GenBank; http://www.ncbi.nlm.nih.gov/genbank): AF065933.1 (*CCL2*), AF128218.1 (*CCL4*), AF128196.1 (*CCL9*), U50712.1 (*CCL12*), NM_011332.1 (*CCL17*), AF099052.1 (*CCL20*), NM_009138.1 (*CCL25*), NM_020279.1 (*CCL28*), NM_008176.1 (*CXCL1*), NM_009140.1 (*CXCL2*), NM_009141.1 (*CXCL5*), NM_008599.1 (*CXCL9*), NM_021274.1 (*CXCL10*), and AF252873.1 (*CXCL14*).

Quantitative real-time PCR analysis. Murine epidermal sheets were homogenized in liquid nitrogen using a Mikro-Dismembrator U (Braun Biotech). Total RNA was extracted from Pam-212 keratinocytes or homogenized epidermis using ISOGEN (Nippon Gene), and cDNA was synthesized using the SuperScript system (Invitrogen Life Technologies). Subsequently, relative mRNA expression was determined by real-time PCR using an ABI PRISM 5500 Sequence Detection System (Applied Biosystems) with SYBR Green I Dye (Qiagen). Primers corresponding to mouse chemokines, TGF-β, and G3PDH were designed by TAKARA BIO INC. Ct numbers were derived from the exponential phase of PCR amplification. Fold differences in the expression of gene *x* in the cell populations *y* and *z* were derived by the formula 2^k, where $k = (Ctx - CtG3PDH)y - (Ctx - CtG3PDH)z$.

Measurement of TGF-β production and its activity in mucosa and skin. To measure TGF-β production, skin and mucosa samples were taken from the trunk and the large or small intestine of ZA and ZD mice. The pieces of cutaneous (1.0×1.0 cm^2) or mucosal (100 mg) tissues were cultured with the epithelial side upward in 24-well plates containing 2 ml RPMI medium (Invitrogen), with 10% FCS, 10 mM HEPES, 0.25 μg/ml gentamicin, and 2 mM L-glutamine for 24 hours. TGF-β production in culture supernatants was measured by ELISA (R&D Systems). In general, TGF-β is secreted in a latent complex in which TGF-β homodimers are noncovalently associated with homodimers of the propeptide called the latency-associated peptide (LAP), and the release of TGF-β from its LAP is required for binding of TGF-β to the cellular receptors (55). To determine TGF-β activity, we used a bioassay using MFB-F11 cells stably transfected with the reporter plasmid containing 12 CAGA boxes (Smad-binding element) fused to a SEAP

reporter gene (56). Briefly, MFB-F11 cells (4×10^4 cells/well) in 96-well flat-bottom tissue culture plates were incubated in 50 μl serum-free DMEM for 2 hours, and then skin culture supernatants or TGF-β (10 pg/ml) were added in a 50 μl volume in the presence or absence of 10 μM HTS466284. After 24 hours of incubation, SEAP activity in the culture supernatants was measured using Gene Light 55 (Microtec).

Statistics. Significant differences between experimental groups were analyzed by Student's *t* test (1 tailed). *P* values less than 0.05 were considered significant.

Study approval. The murine studies were conducted with the approval of and in accordance with the Guidelines for Animal Experiments of the University of Yamanashi. The human study protocol was approved by the institutional review boards of the University Hospital (University of Yamanashi), and informed consent was obtained from all subjects.

Acknowledgments

We thank Takamitsu Matsuzawa, Rui Aoki, Miyuki Ogino, and Kayoko Ohshimo for technical assistance and Kazutoshi Harada and Naotaka Shibagaki for helpful discussions. We thank Akashi Izumi and Shigeo Ihara for their help with microarray analysis. These studies were supported in part by a grant from the Ministry of Education and Science of the Japanese Government.

Received for publication April 20, 2011, and accepted in revised form November 16, 2011.

Address correspondence to: Tatsuyoshi Kawamura, 1110 Shimokato, Chuo, Yamanashi 409-3898, Japan. Phone: 81.55.273.6766; Fax: 81.55.273.6766; E-mail: tkawa@yamanashi.ac.jp.

1. Prasad AS. Zinc: an overview. *Nutrition.* 1995; 11(1 suppl):93–99.
2. Vallee BL, Auld DS. Cocatalytic zinc motifs in enzyme catalysis. *Proc Natl Acad Sci U S A.* 1993; 90(7):2715–2718.
3. Brown KH, Peerson JM, Rivera J, Allen LH. Effect of supplemental zinc on the growth and serum zinc concentrations of prepubertal children: a meta-analysis of randomized controlled trials. *Am J Clin Nutr.* 2002;75(6):1062–1071.
4. Kitamura H, et al. Toll-like receptor-mediated regulation of zinc homeostasis influences dendritic cell function. *Nat Immunol.* 2006;7(9):971–977.
5. Yamasaki S, et al. Zinc is a novel intracellular second messenger. *J Cell Biol.* 2007;177(4):637–645.
6. Haase H, et al. Zinc signals are essential for lipopolysaccharide-induced signal transduction in monocytes. *J Immunol.* 2008;181(9):6491–6502.
7. Kabu K, et al. Zinc is required for Fc epsilon RI-mediated mast cell activation. *J Immunol.* 2006; 177(2):1296–1305.
8. Maverakis E, et al. Acrodermatitis enteropathica and an overview of zinc metabolism. *J Am Acad Dermatol.* 2007;56(1):116–124.
9. Kury S, et al. Identification of SLC39A4, a gene involved in acrodermatitis enteropathica. *Nat Genet.* 2002;31(3):239–240.
10. Wang K, Zhou B, Kuo YM, Zemansky J, Gitschier J. A novel member of a zinc transporter family is defective in acrodermatitis enteropathica. *Am J Hum Genet.* 2002;71(1):66–73.
11. Kury S, et al. Mutation spectrum of human SLC39A4 in a panel of patients with acrodermatitis enteropathica. *Hum Mutat.* 2003;22(4):337–338.
12. Maggini S, Wenzlaff S, Hornig D. Essential role of vitamin C and zinc in child immunity and health. *J Int Med Res.* 2010;38(2):386–414.
13. Song Y, et al. Dietary zinc restriction and repletion affects DNA integrity in healthy men. *Am J Clin Nutr.* 2009;90(2):321–328.
14. Rink L, Haase H. Zinc homeostasis and immunity. *Trends Immunol.* 2007;28(1):1–4.
15. Murakami M, Hirano T. Intracellular zinc homeostasis and zinc signaling. *Cancer Sci.* 2008; 99(8):1515–1522.
16. Shankar AH, Prasad AS. Zinc and immune function: the biological basis of altered resistance to infection. *Am J Clin Nutr.* 1998;68(2 suppl):447S–463S.
17. Prasad AS. Effects of zinc deficiency on Th1 and Th2 cytokine shifts. *J Infect Dis.* 2000; 182(suppl 1):S62–S68.
18. Prasad AS, et al. Serum thymulin in human zinc deficiency. *J Clin Invest.* 1988;82(4):1202–1210.
19. Richter M, Cantin AM, Beaulieu C, Cloutier A, Larivee P. Zinc chelators inhibit eotaxin, RANTES, and MCP-1 production in stimulated human airway epithelium and fibroblasts. *Am J Physiol Lung Cell Mol Physiol.* 2003;285(3):L719–L729.
20. Zhou Z, Wang L, Song Z, Saari JT, McClain CJ, Kang YJ. Abrogation of nuclear factor-kappaB activation is involved in zinc inhibition of lipopolysaccharide-induced tumor necrosis factor-alpha production and liver injury. *Am J Pathol.* 2004;164(5):1547–1556.
21. von Bulow V, et al. Zinc-dependent suppression of TNF-alpha production is mediated by protein kinase A-induced inhibition of Raf-1, I kappa B kinase beta, and NF-kappa B. *J Immunol.* 2007;179(6):4180–4186.
22. von Bulow V, Rink L, Haase H. Zinc-mediated inhibition of cyclic nucleotide phosphodiesterase activity and expression suppresses TNF-alpha and IL-1 beta production in monocytes by elevation of guanosine 3′,5′-cyclic monophosphate. *J Immunol.* 2005;175(7):4697–4705.
23. King LE, Fraker PJ. Zinc deficiency in mice alters myelopoiesis and hematopoiesis. *J Nutr.* 2002; 132(11):3301–3307.
24. Fraker PJ, King LE, Laakko T, Vollmer TL. The dynamic link between the integrity of the immune system and zinc status. *J Nutr.* 2000;130(5S suppl):1399S–1406S.
25. Lazarowski ER, Boucher RC, Harden TK. Mechanisms of release of nucleotides and integration of their action as P2X- and P2Y-receptor activating molecules. *Mol Pharmacol.* 2003;64(4):785–795.
26. Mizumoto N, Mummert ME, Shalhevet D, Takashima A. Keratinocyte ATP release assay for testing skin-irritating potentials of structurally diverse chemicals. *J Invest Dermatol.* 2003;121(5):1066–1072.
27. Koizumi S, Fujishita K, Inoue K, Shigemoto-Mogami Y, Tsuda M. Ca2+ waves in keratinocytes are transmitted to sensory neurons: the involvement of extracellular ATP and P2Y2 receptor activation. *Biochem J.* 2004;380(pt 2):329–338.
28. Mizumoto N, et al. CD39 is the dominant Langerhans cell-associated ecto-NTPDase: modulatory roles in inflammation and immune responsiveness. *Nat Med.* 2002;8(4):358–365.
29. Koizumi S, Fujishita K, Inoue K. Regulation of cell-to-cell communication mediated by astrocytic ATP in the CNS. *Purinergic Signal.* 2005;1(3):211–217.
30. Grabbe S, Schwarz T. Immunoregulatory mechanisms involved in elicitation of allergic contact hypersensitivity. *Immunol Today.* 1998;19(1):37–44.
31. Zhang L, Tinkle SS. Chemical activation of innate and specific immunity in contact dermatitis. *J Invest Dermatol.* 2000;115(2):168–176.
32. Meller S, et al. Chemokine responses distinguish chemical-induced allergic from irritant skin inflammation: memory T cells make the difference. *J Allergy Clin Immunol.* 2007;119(6):1470–1480.
33. Olson TS, Ley K. Chemokines and chemokine receptors in leukocyte trafficking. *Am J Physiol Regul Integr Comp Physiol.* 2002;283(1):R7–R28.
34. Ohara H, et al. Gene expression profiling defines the role of ATP-exposed keratinocytes in skin inflammation. *J Dermatol Sci.* 2010;58(2):143–151.
35. Merad M, Ginhoux F, Collin M. Origin, homeostasis and function of Langerhans cells and other langerin-expressing dendritic cells. *Nat Rev Immunol.* 2008;8(12):935–947.
36. Borkowski TA, Letterio JJ, Farr AG, Udey MC. A role for endogenous transforming growth factor beta 1 in Langerhans cell biology: the skin of transforming growth factor beta 1 null mice is devoid of epidermal Langerhans cells. *J Exp Med.* 1996;184(6):2417–2422.
37. Tesseur I, Zou K, Berber E, Zhang H, Wyss-Coray T. Highly sensitive and specific bioassay for measuring bioactive TGF-beta. *BMC Cell Biol.* 2006;7:15.
38. Riedl E, Strobl H, Majdic O, Knapp W. TGF-beta 1 promotes in vitro generation of dendritic cells by protecting progenitor cells from apoptosis. *J Immunol.* 1997;158(4):1591–1597.
39. Ohtani T, et al. TGF-beta1 dampens the susceptibility of dendritic cells to environmental stimulation, leading to the requirement for danger signals for activation. *Immunology.* 2009;126(4):485–499.
40. Wilson D, Varigos G, Ackland ML. Apoptosis may underlie the pathology of zinc-deficient skin. *Immunol Cell Biol.* 2006;84(1):28–37.
41. Kaplan DH, Jenison MC, Saeland S, Shlomchik WD, Shlomchik MJ. Epidermal langerhans cell-deficient mice develop enhanced contact hypersensitivity. *Immunity.* 2005;23(6):611–620.
42. Kissenpfennig A, et al. Dynamics and function of Langerhans cells in vivo: dermal dendritic cells colonize lymph node areas distinct from slower migrating Langerhans cells. *Immunity.* 2005;22(5):643–654.
43. Bennett CL, et al. Inducible ablation of mouse Langerhans cells diminishes but fails to abrogate contact hypersensitivity. *J Cell Biol.* 2005;169(4):569–576.
44. Honda T, et al. Compensatory role of Langerhans cells and langerin-positive dermal dendritic cells in the sensitization phase of murine contact hypersensitivity. *J Allergy Clin Immunol.* 2010;125(5):1154–1156.
45. Chai F, Truong-Tran AQ, Evdokiou A, Young GP, Zalewski PD. Intracellular zinc depletion induces caspase activation and p21 Waf1/Cip1 cleavage in human epithelial cell lines. *J Infect Dis.* 2000; 182(suppl 1):S85–S92.
46. Kolenko V, et al. Dead or dying: necrosis versus apoptosis in caspase-deficient human renal cell carcinoma. *Cancer Res.* 1999;59(12):2838–2842.
47. Kim SJ, Jeang KT, Glick AB, Sporn MB, Roberts AB. Promoter sequences of the human transforming growth factor-beta 1 gene responsive to transforming growth factor-beta 1 autoinduction. *J Biol Chem.* 1989;264(12):7041–7045.
48. Kaplan DH, Li MO, Jenison MC, Shlomchik WD, Flavell RA, Shlomchik MJ. Autocrine/paracrine TGF-beta1 is required for the development of epidermal Langerhans cells. *J Exp Med.* 2007;204(11):2545–2552.
49. Luo Y, Hu W, Xu R, Hou B, Zhang L, Zhang W. ZNF580, a novel C2H2 zinc finger transcription factor, interacts with TGF-beta signal molecule SMAD2. *Cell Biol Int.* 2011;35(11):1153–1157.
50. Hacker C, et al. Transcriptional profiling identifies Id2 function in dendritic cell development. *Nat Immunol.* 2003;4(4):380–386.

51. Chai F, Truong-Tran AQ, Ho LH, Zalewski PD. Regulation of caspase activation and apoptosis by cellular zinc fluxes and zinc deprivation: A review. *Immunol Cell Biol.* 1999;77(3):272–278.
52. Denda M, Inoue K, Fuziwara S, Denda S. P2X purinergic receptor antagonist accelerates skin barrier repair and prevents epidermal hyperplasia induced by skin barrier disruption. *J Invest Dermatol.* 2002;119(5):1034–1040.
53. Kawamura T, Azuma M, Kayagaki N, Shimada S, Yagita H, Okumura K. Fas/Fas ligand-mediated apoptosis of murine Langerhans cells. *J Dermatol Sci.* 2000;22(2):96–101.
54. Ogawa Y, Kawamura T, Kimura T, Ito M, Blauvelt A, Shimada S. Gram-positive bacteria enhance HIV-1 susceptibility in Langerhans cells, but not in dendritic cells, via Toll-like receptor activation. *Blood.* 2009;113(21):5157–5166.
55. Schmierer B, Hill CS. TGFbeta-SMAD signal transduction: molecular specificity and functional flexibility. *Nat Rev Mol Cell Biol.* 2007;8(12):970–982.
56. Nakamura Y, et al. House dust mite allergen Der f 1 can induce the activation of latent TGF-beta via its protease activity. *FEBS Lett.* 2009;583(12):2088–2092.

OPEN ACCESS Freely available online

PLoS one

K70Q Adds High-Level Tenofovir Resistance to "Q151M Complex" HIV Reverse Transcriptase through the Enhanced Discrimination Mechanism

Atsuko Hachiya[1,2], Eiichi N. Kodama[3]*, Matthew M. Schuckmann[1], Karen A. Kirby[1], Eleftherios Michailidis[1], Yasuko Sakagami[4], Shinichi Oka[2], Kamalendra Singh[1], Stefan G. Sarafianos[1]*

1 Department of Molecular Microbiology and Immunology, University of Missouri School of Medicine, Columbia, Missouri, United States of America, **2** AIDS Clinical Center, National Center for Global Health and Medicine, Tokyo, Japan, **3** Division of Emerging Infectious Diseases, Tohoku University School of Medicine, Sendai, Japan, **4** Institute for Virus Research, Kyoto University, Kyoto, Japan

Abstract

HIV-1 carrying the "Q151M complex" reverse transcriptase (RT) mutations (A62V/V75I/F77L/F116Y/Q151M, or Q151Mc) is resistant to many FDA-approved nucleoside RT inhibitors (NRTIs), but has been considered susceptible to tenofovir disoproxil fumarate (TFV-DF or TDF). We have isolated from a TFV-DF-treated HIV patient a Q151Mc-containing clinical isolate with high phenotypic resistance to TFV-DF. Analysis of the genotypic and phenotypic testing over the course of this patient's therapy lead us to hypothesize that TFV-DF resistance emerged upon appearance of the previously unreported K70Q mutation in the Q151Mc background. Virological analysis showed that HIV with only K70Q was not significantly resistant to TFV-DF. However, addition of K70Q to the Q151Mc background significantly enhanced resistance to several approved NRTIs, and also resulted in high-level (10-fold) resistance to TFV-DF. Biochemical experiments established that the increased resistance to tenofovir is not the result of enhanced excision, as K70Q/Q151Mc RT exhibited diminished, rather than enhanced ATP-based primer unblocking activity. Pre-steady state kinetic analysis of the recombinant enzymes demonstrated that addition of the K70Q mutation selectively decreases the binding of tenofovir-diphosphate (TFV-DP), resulting in reduced incorporation of TFV into the nascent DNA chain. Molecular dynamics simulations suggest that changes in the hydrogen bonding pattern in the polymerase active site of K70Q/Q151Mc RT may contribute to the observed changes in binding and incorporation of TFV-DP. The novel pattern of TFV-resistance may help adjust therapeutic strategies for NRTI-experienced patients with multi-drug resistant (MDR) mutations.

Citation: Hachiya A, Kodama EN, Schuckmann MM, Kirby KA, Michailidis E, et al. (2011) K70Q Adds High-Level Tenofovir Resistance to "Q151M Complex" HIV Reverse Transcriptase through the Enhanced Discrimination Mechanism. PLoS ONE 6(1): e16242. doi:10.1371/journal.pone.0016242

Editor: Zandrea Ambrose, University of Pittsburgh, United States of America

Received September 15, 2010; **Accepted** December 8, 2010; **Published** January 13, 2011

Funding: This work was supported by a grant for the promotion of AIDS Research from the Ministry of Health, Labor and Welfare (AH and EK, http://www.mhlw.go.jp/english/index.html), by grants from the Korea Food & Drug Administration and the Ministry of Knowledge and Economy, Bilateral International Collaborative R&D Program, Republic of Korea (SGS) and by National Institutes of Health (NIH, http://nih.gov/) research grants AI094715, AI076119, AI079801, and AI074389 to SGS. The funders had no role in study design, data collection and analysis, decision to publish, or preparation of the manuscript.

Competing Interests: The authors have declared that no competing interests exist.

* E-mail: sarafianoss@missouri.edu (SGS); kodama515@m.tains.tohoku.ac.jp (ENK)

Introduction

Nucleos(t)ide reverse transcriptase inhibitors (NRTIs) are used in combination with other classes of drugs for the treatment of patients infected with human immunodeficiency virus type-1 (HIV-1). This approach is known as highly active anti-retroviral therapy (HAART) and has been remarkably successful in reducing the viral loads and increasing the number of CD4+ cells in patients' plasma. However, prolonged therapies inevitably result in resistance to all of the available drugs. Several mutations in the reverse transcriptase (RT) are known to cause resistance to NRTIs through two basic mechanisms:

1) The excision mechanism, which is based on an enhanced capacity of RT to use adenosine triphosphate (ATP) as a nucleophile for the removal of the chain-terminating nucleotide from the DNA terminus. The excision reaction products are a 5′, 5′-dinucleoside tetraphosphate and an unblocked primer with a free 3′-OH, allowing DNA synthesis to resume [1,2,3]. Increased excision of NRTIs is imparted by Excision Enhancement Mutations, typically M41L, D67N, K70R, T215Y/F, L210W, and K219E/Q (also known as Thymidine Associated Mutations, or TAMs). Other mutations have also been reported to enhance excision, including insertions or deletions at the tip of the β3- β4 loop of the fingers subdomain in the background of other excision enhancement mutations [4,5,6,7,8,9,10,11].

2) The other mechanism of NRTI resistance is the exclusion mechanism, which is caused when NRTI-resistance mutations in RT enhance discrimination and reduce incorporation of the NRTI-triphosphate (NRTI-TP). This mechanism is exemplified by the resistance of the M184V RT mutant to lamivudine (3TC) and emtricitabine (FTC) due to steric clash between the β-branched Val or Ile at position 184 and the oxathiolane ring of the inhibitors [12,13]. Another example of the exclusion mechanism is the multi-drug resistant (MDR) HIV-1 RT known as Q151M complex (Q151Mc). This RT contains the Q151M mutation together with a cluster of four

additional mutations (A62V/V75I/F77L/F116Y) [14,15]. Q151M by itself causes intermediate- to high-level resistance to zidovudine (AZT), didanosine (ddI), zalcitabine (ddC), stavudine (d4T), and low level resistance to abacavir (ABC) [15,16,17] without reducing viral fitness [18,19]. Addition of the four associated mutations increases replication capacity of RT and results in high-level resistance to AZT, ddI, ddC, and d4T, 5-fold resistance to ABC and low-level resistance to lamivudine (3TC) and emtricitabine (FTC) [17,18,19,20,21]. Miller *et al.* and Smith *et al.* reported a 1.8-fold and 3.6-fold increase in resistance to tenofovir (TFV), respectively [22,23].

Biochemical studies on the mechanism of Q151Mc resistance to multiple NRTIs have revealed that the mutations of this complex decrease the maximum rate of NRTI-TP incorporation without significantly affecting the incorporation of the natural nucleotides [21,24,25]. Structurally, the Q151 residue interacts with the 3′-OH of a normal deoxynucleoside triphosphate (dNTP) substrate [26]. It appears that the Q151Mc mutations cause resistance to multiple NRTIs by affecting the hydrogen bond network involving protein side chains in the vicinity of the dNTP-binding site and the NRTI triphosphate lacking a 3′-OH [25,26,27]. The Q151Mc set of mutations was also reported to decrease pyrophosphate PPi- and ATP-mediated excision [25].

K65R is another mutation near the polymerase active site that confers NRTI resistance through the exclusion mechanism. Specifically, K65R RT has reduced susceptibility to the acyclic nucleotide analog, TFV and other NRTIs, including ddI, ddC, ABC, FTC and 3TC [28,29,30,31]. Biochemical studies with K65R RT have demonstrated that this enzyme decreases the incorporation rate of these NRTIs [32,33,34]. The crystal structure of K65R RT in complex with DNA and TFV diphosphate (TFV-DP) revealed that R65 forms a molecular platform with the conserved residue R72, and the platform enhances the ability of K65R RT to discriminate NRTIs from dNTPs [35]. HIV carrying the Q151Mc mutations has been reported to be susceptible to TFV disoproxil fumarate (TFV-DF), the oral prodrug of TFV that enhances its oral bioavailability and anti-HIV activity [22,36]. While the K65R mutation appeared in several patients treated for more than 18 months with TFV-DF, no patient developed multi-NRTI resistance through appearance of Q151Mc [37].

Here we report the identification of unique HIV clinical isolates that have acquired the K70Q mutation in the background of Q151Mc during TFV-DF-containing therapy. We have used a combination of virological, biochemical, and molecular modeling methods to derive the mechanism by which this mutation confers resistance to TFV.

Materials and Methods

Clinical samples

HIV was isolated from fresh plasma immediately after collection of clinical samples from study participants at the outpatient clinic of the AIDS Clinical Center (ACC), International Medical Center of Japan. The Institutional Review Board approved this study (IMCJ-H13-80) and a written consent was obtained from all participants.

Construction of recombinant clones of HIV-1

Recombinant infectious clones of HIV-1 carrying various mutations were prepared using standard site-directed mutagenesis protocols as described previously [38]. The NL4-3-based molecular clone was constructed by replacing the *pol*-coding region with the HIV-1 BH10 strain. Restriction enzyme sites *Xma I* and *Nhe I* were introduced by silent mutations into the molecular clone at positions corresponding to HIV-1 RT codons 15 and 267, respectively [39]. Each molecular clone was transfected into COS-7 cells. Cells were grown for 48 h, and culture supernatants were harvested and stored at −80°C until use.

Single-cycle drug susceptibility assay

Susceptibilities to various RT inhibitors were determined using the MAGIC-5 cells which are HeLa cells stably transfected with a β-galactosidase gene under the control of an HIV long terminal repeat promoter, and with vectors that express the CD4 receptor and the CCR5 co-receptor under the control of the CMV promoter as described previously [40]. Briefly, MAGIC-5 cells were infected with diluted virus stock (100 blue forming units) in the presence of increasing concentrations of RT inhibitors, cultured for 48 h, fixed, and stained with X-Gal (5-bromo-4-chloro-3-indolyl-β-D-galacto-pyranoside). The stained cells were counted under a light microscope. Drug concentrations reducing the number of infected cells to 50% of the drug-free control (EC_{50}) were determined from dose response curves.

Enzymes

RT sequences coding for the p66 and p51 subunits of BH10 were cloned in the pRT dual vector, which is derived from pCDF-2 with LIC duet minimal adaptor (Novagen), using restriction sites *PpuMI* and *SacI* for the p51 subunit, and *SacII* and *AvrII* for the p66 subunit. RT was expressed in the *Escherichia coli* strain BL21 (Invitrogen) and purified by nickel affinity chromatography and MonoQ anion exchange chromatography [41]. RT concentrations were determined spectrophotometrically based on absorption at 260 nm using a calculated extinction coefficient (261,610 M^{-1} cm^{-1}). The active site concentration of the various RT preparations was calculated as described below.

Nucleic acid substrates

DNA oligomers were synthesized by Integrated DNA Technologies (Coralville, IA). An 18-nucleotide DNA primer fluorescently labeled with Cy3 at the 5′ end (P_{18}; 5′-Cy3 GTC CCT GTT CGG GCG CCA-3′) and a 100-nucleotide DNA template (T_{100}; 5′-TAG TGT GTG CCC GTC TGT TGT GTG ACT CTG GTA ACT AGA GAT CCC TCA GAC CCT TTT AGT CAG TGT GGA AAA TCT CTA GCA GTG GCG CCC GAA CAG GGA C-3′) were used in primer extension assays. An 18-nucleotide DNA primer 5′-labeled with Cy3 (P_{18}; 5′-Cy3 GTC ACT GTT CGA GCA CCA-3′) and a 31-nucleotide DNA template (T_{31}; 5′- CCA TAG CTA GCA TTG GTG CTC GAA CAG TGA C-3′) were used in the ATP rescue assay and pre-steady state kinetic experiments.

Active site titration and determination of the dissociation constant for DNA binding ($K_{D\text{-}DNA}$)

Determination of active site concentrations in the different preparations of WT and mutant RTs were performed using pre-steady state burst experiments. A fixed concentration of RT (80 nM, determined by absorbance measurements) was pre-incubated with increasing concentrations of DNA/DNA template/primer (T_{31}/P_{18}), followed by rapidly mixing with a reaction mixture containing $MgCl_2$ and dATP, at final concentrations of 5 mM and 50 μM, respectively. The reactions were quenched at various times (10 ms to 5 s) by adding EDTA to a final concentration of 50 mM. The amounts of product (P_{18}-dAMP) were quantitated and fit to the following burst equation:

$$P = A\left(1 - e^{-kobst}\right) + k_{ss}t \quad (1)$$

where A is the amplitude of the burst phase that represents the RT-DNA complex at the start of the reaction, k_{obs} is the observed burst rate constant for dNTP incorporation, k_{ss} is the steady state rate constant, and t is the reaction time. The rate constant of the linear phase (k_{cat}) can be estimated by dividing the slope of the linear phase by the enzyme concentration. The active site concentration and template/primer binding affinity ($K_{D\text{-}DNA}$) were determined by plotting the amplitude (A) against the concentration of template/primer. The data were fit using non-linear regression to a quadratic equation:

$$A = 0.5(K_D + [RT] + [DNA]) - \sqrt{0.25(K_D + [RT] + [DNA])^2 - ([RT][DNA])} \quad (2)$$

where K_D is the dissociation constant for the RT-DNA complex, and [RT] is the concentration of active polymerase molecules. Subsequent biochemical experiments were performed using corrected active site concentrations [42,43].

Primer extension assay

To examine the DNA polymerase activity of WT and mutant RTs and the inhibition of DNA synthesis by TFV, the primer extension assays were carried out on the T_{100}/P_{18} template/primer (P_{18} was 5′-Cy3 labeled) in the presence or absence of 3.5 mM ATP [41]. The enzyme (20 nM active sites) was incubated with 20 nM template/primer at 37°C in a buffer containing 50 mM Tris-HCl, pH 7.8 and 50 mM NaCl. The DNA synthesis was initiated by the addition of 1 μM dNTP and 10 mM $MgCl_2$. The primer extension assays were carried out in the presence or absence of varying concentrations of TFV-DP. The reactions were terminated after 15 min by adding equal volume of 100% formamide containing traces of bromophenol blue. The extension products were resolved on a 7 M urea-15% polyacrylamide gel, and visualized by phosphor-imaging (FLA 5100, Fujifilm, Tokyo). We followed standard protocols that utilize the Multi Gauge software (Fujifilm) to quantitate primer extension [41,44]. The results from dose response experiments were plotted using Prism 4 (GraphPad Software Inc., CA) and IC_{50} values for TFV-DP were obtained at midpoint concentrations.

ATP-dependent rescue assay

Template/primer (T_{31}/P_{18}) terminated with TFV (T/P_{TFV}) was prepared as described in Michailidis et al [41]. 20 nM of T/P_{TFV} was incubated at 37°C with HIV-1 RT (60 nM), either at various concentrations of ATP (0–7 mM) for 30 minutes, or for various times (0–120 minutes) with 3.5 mM ATP, in RT buffer containing 50 mM Tris-HCl, pH 7.8, and 50 mM NaCl, and 10 mM $MgCl_2$. The assay was performed in the presence of excess competing dATP (100 μM) that prevented reincorporation of the excised TFV, 0.5 μM dTTP and 10 μM ddGTP. Reactions were quenched with 100% formamide containing traces of bromophenol blue and analyzed as described above. The dissociation constants (K_d) of the various enzymes for ATP used in the rescue reactions were determined by fitting the rescue data at various ATP concentrations, using non-linear regression fitting to hyperbola.

Kinetics of dNTP incorporation by WT and mutant enzymes

To determine the binding affinity of WT and mutant enzymes to the dNTP substrate ($K_{D\text{-}dNTP}$) and to estimate the maximum rate of dNTP incorporation by these enzymes (k_{pol}), we carried out transient-state experiments using a rapid quench instrument (RQF-3, Kintek Corporation, Clarence, PA) at 37°C in RT buffer (50 mM Tris-HCl, pH 7.8 and 50 mM NaCl). HIV-1 RT (50 nM active sites) was pre-incubated with 50 nM T_{31}/P_{18} in one syringe (Syringe A), whereas varying concentrations of dNTP and 10 mM $MgCl_2$ were kept in another syringe (Syringe B). The solutions were rapidly mixed to initiate reactions, which were subsequently quenched at various times (5 ms to 10 s) by adding EDTA to a final concentration of 50 mM. The products from each quenched reaction were resolved, quantitated, and plotted as described above. The data were fit by non-linear regression to the burst equation (Eq 1).

To obtain the dissociation constant $K_{D\text{-}dNTP}$ for dNTP binding to the RT-DNA complex, the observed burst rates (k_{obs}) were fit to the hyperbolic equation (Eq. 3) using nonlinear regression:

$$k_{obs} = \left(k_{pol}[dNTP]\right)/(K_{D-dNTP} + [dNTP]) \quad (3)$$

where k_{pol} is the optimal rate of dNTP incorporation.

The kinetics of TFV incorporation by the WT and mutant enzymes were carried out in a manner similar to that employed for natural dNTP substrate except the time of reactions. It was noted that the mutant enzymes required longer time to incorporate TFV compared to the WT HIV-1 RT (detailed in the Results section).

Molecular Modeling

Molecular models of mutant enzymes were generated using SYBYL (Tripos Associates, St. Louis, MO). The starting protein coordinates were from the crystal structure of HIV-1 RT in complex with DNA template/primer and TFV-DP (PDB file 1T05) [45]. They were initially modified by the Protein Preparation tool (Schrodinger Molecular Modeling Suit, NY), which deletes unwanted water molecules, sets charges and atom type of metal ions, corrects misoriented Gln and Asn residues, and optimizes H-atom orientations. Amino acid side chains were substituted in by Maestro (Schrodinger, Molecular Modeling Suite, NY). Molecular dynamics simulations of the WT and mutant RT models were carried out to obtain the most stable structures by Impact, interfaced with Maestro at constant temperature, and OPLS_2005 force field. The molecular dynamics simulations were performed for 1000 steps with 0.001 ps intervals. The temperature relaxation time was 0.01 ps. The Verlet integration algorithm was used in simulations. The structures were imported into Pymol (http://www.pymol.org) for visualization and comparison.

Results

Phenotypic resistance to TFV-DF in the absence of any known TFV resistance mutations

During phenotypic and genotypic evaluation of the clinical isolates we identified a unique virus that exhibited an apparent discordance between the phenotypic and genotypic results. The clinical history of the patient and the corresponding genotypic and phenotypic changes during the course of the therapy are summarized in Fig. 1. (Also see Table S1). The patient's treatment before Feb 2002 included d4T, ddI, and EFV and did not decrease significantly the viral loads (Fig 1A). Hence, the therapeutic regimen was switched to TFV-DF, EFV, and the protease inhibitor lopinavir (LPV). However, the patient's immunological and virological responses still did not improve due to poor adherence, especially to LPV. Genotypic and phenotypic analyses on March 2002 (point 1) and June 2002 (point 2) revealed

A

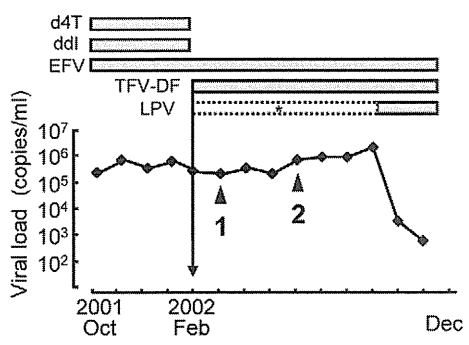

B

Phenotypic profile

Isolate	Fold increase in EC_{50}								
	AZT	ddI	d4T	3TC	ABC	**TFV·DF**	FTC	NVP	EFV
1	61	12	9	13	10	**2**	9	>200	>500
2	57	>40	>50	31	15	**6**	5	>200	>500

C

Genotypic profile

Isolate	Resistance-associated mutation		Other newly acquired mutations
	NRTI	NNRTI	
1	Q151M complex, V106M, V179D		-
2	Q151M complex, V106M, V179D, V108I		**K70Q**, K102R

Figure 1. Clinical course of patient and drug resistance profile. (A) The two clinical isolates were collected from the patient at the time points indicated by triangles. Both isolates had no known resistant mutations in the protease region. During the period indicated by asterisk, LPV was administrated but the patient demonstrated poor adherence due to undesirable side effects. After instruction on the use of antiretroviral drugs, the viral loads successfully decreased below the detection limit (<50 copies/ml). (B) Phenotypic drug susceptibility assays of clinical isolates in at least three independent experiments are shown as a relative increase in EC_{50} compared to HIV-1 NL4-3 strain which served as WT (see also Table S1). (C) Mutations observed in the isolates that are defined as the NRTI and NNRTI resistance associated mutations deposited in the HIV Drug Resistance Database maintained by International AIDS Society 2009 [58] and the Stanford University (http://hivdb.stanford.edu/) were shown. Abbreviations of drugs used: d4T, stavudine; ddI, didenosine; EFV, efavirenz; TFV-DF, tenofovir disoproxil fumarate; LPV, lopinovir; AZT, zidovudine; 3TC, lamivudine; ABC, abacavir; FTC, emtricitabine; NVP, nevirapine.
doi:10.1371/journal.pone.0016242.g001

resistance to multiple RT inhibitors, including NNRTIs (Fig 1B). Resistance to all NRTIs, except AZT and FTC, was enhanced in the point 2 isolate (Fig. 1B). Notably, this isolate showed an increase in resistance to TFV-DF in the absence of the canonical TFV resistance mutation (K65R) and in the presence of Q151Mc mutations (Fig. 1C). Previously, it has been shown that Q151Mc remains susceptible to TFV [22] although Smith *et al.* reported that Q151Mc had a 3.6-fold increase in TFV resistance [23]. Suppression of the viral load was finally achieved by improvement in drug adherence to LPV and by the addition of FTC in the therapeutic regimen, since no protease resistance mutations were found within the protease coding region.

To identify the mutation(s) responsible for the unexpected resistance to TFV-DF we sequenced the entire RT coding region at time-points 1 and 2 (Figure S1, GenBank Accession Number AB506802 and AB506803). Of the three substituted residues (70, 102, and 108) amino acids 102 and 108 are part of the structurally distinct NNRTI binding pocket [46], which can mutate during EFV-based therapeutic regimens. However, residue 70 is located in the β3-β4 hairpin loop of the p66 "fingers" subdomain of HIV-1 RT, which interacts with the incoming dNTP substrate [10,27]. Different mutations at this site have been previously implicated in NRTI resistance [47], suggesting that the observed K70Q mutation may be involved in the increased resistance to TFV-DF.

NRTI resistance enhancement by mutation at residue 70

Several mutations at position 70 of HIV-1 RT (R, G, E, T, N and Q) have been reported to the Stanford HIV-1 Drug Resistance Database (http://hivdb.stanford.edu/, accessed on Feb. 27th 2010). K70Q is rarely observed in treatment-naïve patients (0.04%), but appears more often in clinical samples from NRTI-treated patients (0.1%, $p<0.0001$ compared with the frequency of K70Q in treatment-naïve patients) but not NNRTI-treated patients. Furthermore, K70Q is observed in 0.5% of the clinical samples from patients infected with HIV-1 Q151M. There have been no previous reports on a possible role of K70Q in NRTI resistance.

To examine the effect of K70Q on drug susceptibility we generated a series of HIV variants with mutations at RT codon 70 (Figure 2A and also Table S2). The HIV-1_{K70Q} variant exhibited marginal resistance to ddI and 3TC (5- and 3.3-fold, respectively), but no significant resistance to other NRTIs. We further examined whether the mutations at residue 70 affect susceptibility to NRTIs in the Q151Mc background (Figure 2B and also Table S3). HIV-$1_{K70G/Q151Mc}$ had enhanced resistance to d4T (4.6-fold) as compared to HIV-1_{Q151Mc}. Notably, HIV-$1_{K70Q/Q151Mc}$ also showed enhanced resistance to ddI and d4T (2.4- and 4.4-fold, respectively, compared to HIV-1_{Q151Mc}). In addition, HIV-$1_{K70Q/Q151Mc}$ displayed 5-fold increased resistance to TFV-DF compared to HIV-1_{Q151Mc}. Other K70 mutations exhibited little or no resistance to TFV-DF.

Primer Extension and ATP-based Rescue Assays

As mentioned earlier, a key mechanism of NRTI resistance is the excision mechanism, which is based on the enhanced ability of NRTI-resistant enzymes to use ATP for unblocking chain-terminated primers and allow for further DNA synthesis to continue [2,3,48]. To determine whether the K70Q mutation causes TFV resistance through the excision mechanism we measured the susceptibility of WT and mutant RTs to inhibition by TFV in the presence or absence of ATP. In gel-based assays, an enhancement in excision would manifest as an increase in the production of fully extended DNA when 3.5 mM ATP is included in the extension reaction [49,50]. Our extension assays in the absence of ATP (no-excision conditions) showed that addition of the K70Q mutation to Q151Mc HIV-1 RT enhances resistance to TFV-DP. However, this enhancement is not influenced by the presence of ATP (Table 1, Fig. 3A and Figure S2A). In fact, excision enhancement due to the presence of ATP measured as [IC_{50} with ATP]/[IC_{50} without ATP] was similar for all enzymes, including the WT RT (from 2.7-fold to 2.9-fold for WT, K70Q, Q151Mc, and K70Q/Q151Mc RTs) (Table 1). Using a related type of assay, the ATP-mediated rescue assay, we compared the rates by which the WT and mutant RTs unblock TFV-terminated primers and extend products past the point of chain-termination. We find that the ATP-based rescue activity of WT RT is not slower, but 1.5-, 2.5-, and 3-fold faster than that of K70Q, Q151Mc, and K70Q/Q151Mc RTs, respectively (Fig. 3B and Figure S2B). In addition, the ATP-based rescue activity of WT RT was saturated at lower concentrations of ATP than K70Q,

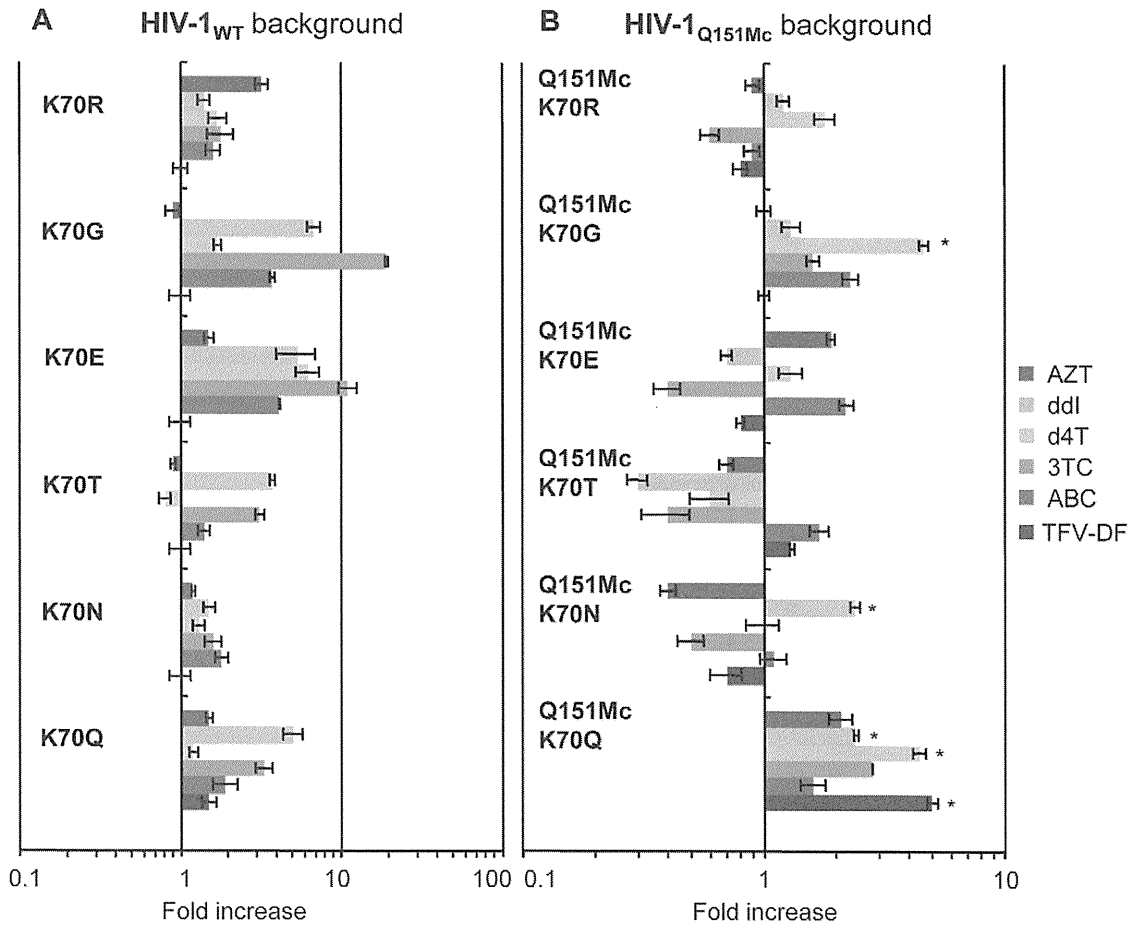

Figure 2. NRTI resistance of HIVs with mutations at RT residue 70 in the background of WT or Q151Mc. Antiviral activities of HIV-1s carrying mutations at residue 70 (K70R, K70G, K70E, K70T, K70N, or K70Q) in the WT (A) or Q151Mc (B) background were determined by the MAGIC5 assay. The data for each clone were compared to WT (A) and Q151Mc (B) HIV-1 and are shown as fold increase; AZT (red), ddI (green), d4T (cyan), 3TC (orange), ABC (blue), and TFV-DF (purple). Error bars represent standard deviations from at least three independent experiments (see also Table S2 and S3). The asterisk indicates statistically significant in EC_{50} values ($P<0.0001$ by t-test).
doi:10.1371/journal.pone.0016242.g002

Table 1. Primer extension assay in the presence or absence of ATP.

Enzyme[a]	IC_{50} (nM) of TFV-DP[b] (fold increase[c])		Excision enhancement due to ATP[d]
	Without ATP	With ATP	
WT	641±83	1854±197	2.9
	(1)[b]	(1)[b]	
K70Q	802±99	2306±270	2.9
	(1.3)	(1.2)	
Q151Mc	1503±90	3996±341	2.7
	(2.3)	(2.1)	
K70Q/Q151Mc	2392±353	7001±226	2.9
	(3.7)	**(3.8)**	

[a]The sequence of HIV RT WT and mutant derived from BH10.
[b]Data are means ± standard deviations from at least three independent experiments.
[c]The relative increase in IC_{50} value compared with each HIV-1 RT WT without, or with ATP is given in parentheses. Bold indicates an increase in fold increase value greater than 3-fold.
[d]Excision enhancement due to ATP is calculated as IC_{50} with ATP/IC_{50} without ATP.
doi:10.1371/journal.pone.0016242.t001

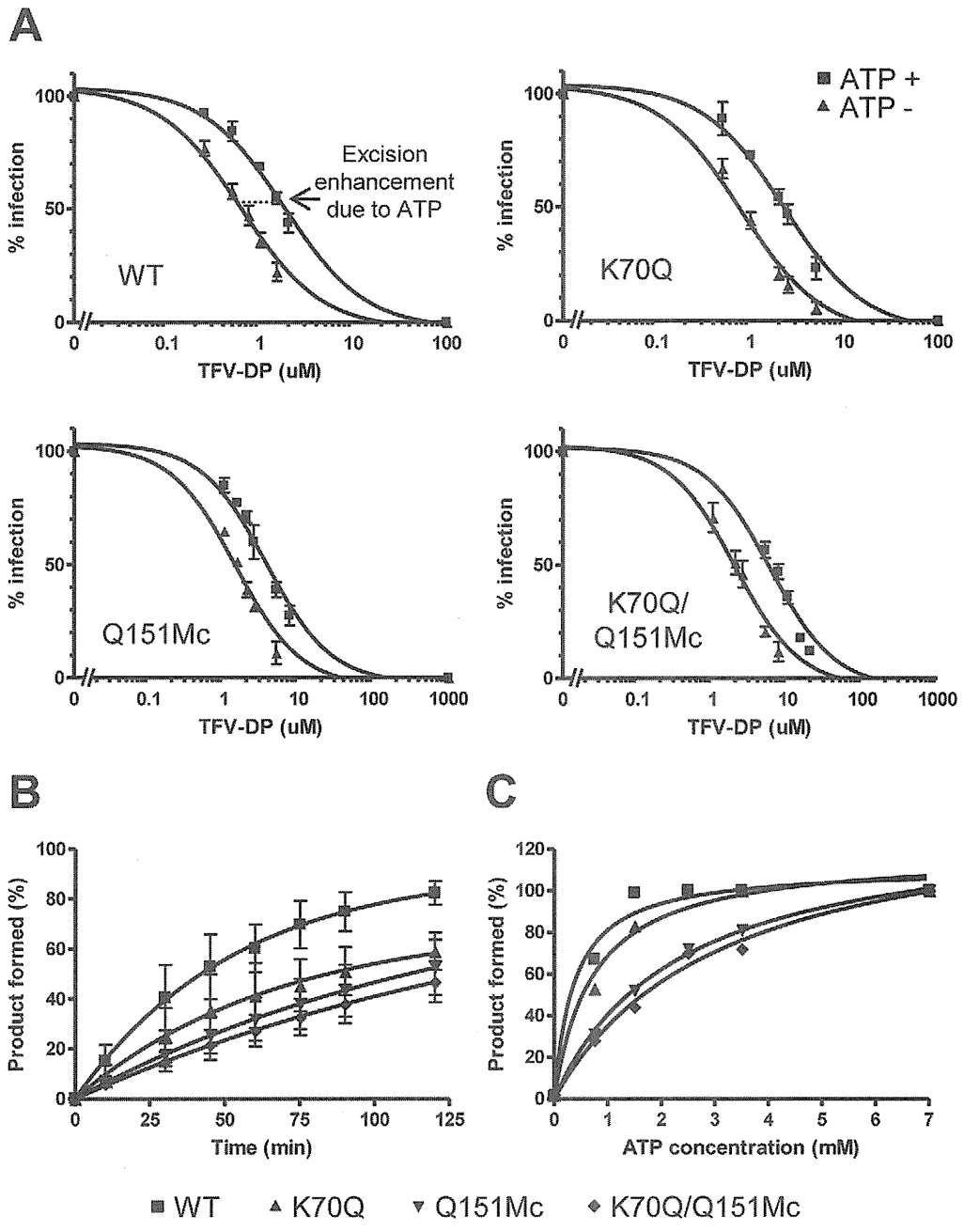

Figure 3. Effects of RT mutations K70Q, Q151Mc, or K70Q/Q151Mc on DNA primer extension activity and on ATP-based excision activities. (A) Effect of varying concentrations of TFV-DP on the primer extension activities of HIV-1 WT and mutant RTs. The experiments were carried out in the presence (■) or absence (▲) of 3.5 mM ATP (B) Time dependence of ATP-based rescue of TFV-terminated primers. TFV-terminated T_{31}/P_{18} oligos (20 nM) were incubated with 60 nM RT and 3.5 mM ATP. The reaction mixture also included excess of competing dATP (100 μM) that prevented reincorporation of TFV-DP and 0.5 μM dTTP, and 10 μM ddGTP that allowed extension of the rescued primer by two nucleotides and chain termination. Rescue products (WT [■], K70Q [▲], Q151Mc [▼] and K70Q/Q151Mc [♦]) were analyzed at indicated time points. (C) ATP-based rescue was dependent on concentration of ATP. Reactions were as in (B), but for 30 minutes and at varying concentrations of ATP. Rescue products at 7 mM ATP are defined as 100% product formed.
doi:10.1371/journal.pone.0016242.g003

Q151Mc, and K70Q/Q151Mc RTs (the apparent $K_{D\text{-}ATP}$ for WT, K70Q, Q151Mc and K70Q/Q151Mc were 0.4, 0.7, 2.3, and 3.1 mM, respectively), suggesting that a better binding of ATP may contribute to the slightly enhanced excision activity of WT RT (Fig. 3C and Figure S2C). Collectively, these results rule out the possibility that K70Q/Q151Mc becomes resistant to TFV through the excision mechanism.

Pre-Steady Kinetic Constants for Binding and Incorporation of dATP and TFV-DP

To determine whether the resistance by K70Q/Q151Mc is caused by an increased preference of physiological dATP substrate over TFV-DP, we carried out pre-steady state transient kinetic analyses of WT, K70Q, Q151Mc, and K70Q/Q151Mc enzymes. The kinetic constants $k_{pol\text{-}dATP}$ and $K_{D\text{-}dATP}$ for WT and mutant

enzymes are presented in Table 2 and Fig. 4 (and also in Figure S3). The results reveal that K70Q, Q151Mc, and K70Q/Q151Mc RTs have increased $k_{pol\text{-}dATP}$ as well as $K_{D\text{-}dATP}$. Both Q151Mc and K70Q/Q151Mc enzymes incorporate dATP faster than WT (17.9 and 14.6 s^{-1}, respectively *vs.* 6.3 s^{-1}) but have a weaker binding affinity for dATP than WT RT (5.4 and 5.0 μM, respectively *vs.* 2.6 μM). Hence, the catalytic efficiency ratio of dATP incorporation remains similar for all enzymes ($k_{pol\text{-}dATP}/K_{D\text{-}dATP}$ ratios for WT, K70Q, Q151Mc, and K70Q/Q151Mc were 2.4, 2.2, 3.3, and 2.9 $\mu M^{-1}\cdot s^{-1}$, respectively). On the contrary, a significant change in the incorporation efficiency of TFV was observed. The K70Q and K70Q/Q151Mc enzymes had more than 4.5-fold reduced affinity for TFV than the WT enzyme ($K_{D\text{-}TFV}$ values were 8.6 and 8.9 μM compared to 1.9 μM). In addition, the turnover rates of TFV incorporation by the WT and K70Q enzymes were comparable ($k_{pol\text{-}TFV}$ were 2.8 and 3.1 s^{-1}, respectively). The addition of the K70Q mutation to Q151Mc also reduced the k_{pol} for TFV-DP. The net effect of these changes was a significant reduction in the TFV-DP incorporation efficiencies of the mutant enzymes compared to the WT enzyme ($k_{pol\text{-}TFV}/K_{D\text{-}TFV}$ ratios for WT, K70Q, Q151Mc, and K70Q/Q151Mc were 1.47, 0.36, 0.3, and 0.11 $\mu M^{-1}\cdot s^{-1}$, respectively; Table 2). WT RT incorporated TFV-DP most efficiently, followed by K70Q>Q151Mc>K70Q/Q151Mc enzymes. As a direct measure of the enzyme's ability to discriminate between the natural dATP substrate and the TFV, we determined the "selectivity", defined as the ratio of efficiency of the enzyme to incorporate dATP over TFV-DP ($k_{pol\text{-}dATP}/K_{D\text{-}dATP}/k_{pol\text{-}TFV}/K_{D\text{-}TFV}$). The selectivity values demonstrate that the K70Q/Q151Mc enzyme favors incorporation of dNTP over TFV-DP 26.3 times compared to 1.6 times by the WT enzyme, leading to a 16.4-fold resistance to TFV (defined as $selectivity_{mutant}/selectivity_{WT}$; Table 2). This resistance is more than twice the TFV resistance of Q151Mc and 4 times the TFV resistance of K70Q.

Molecular modeling

Molecular dynamics simulations on the control structural coordinates of the WT RT/DNA/TFV-DP crystal structure [45] did not cause any significant structural changes, suggesting that the modeling protocols do not alter the structures in ways that are not related to the K70Q or Q151Mc mutations. The root mean square deviation (rmsd) between the Cα atoms of the WT structures before and after simulation was 0.1 Å. Similarly, the rmsd between the Cα atoms of WT and mutant RT molecular models were also very low (~0.1 Å). Comparison of these models showed a significant repositioning of residue 65 in Q151Mc/K70Q (Fig. 5), and to a lesser extent in K70Q or Q151Mc RTs (not shown). Additional smaller changes in the side chains of residues 151, 70, and 72 were also observed (Fig. 5). The structure of TFV-DP was also slightly adjusted, possibly as a result of the changes in the surrounding residues (Fig. 5). While residue 70 is located proximal to residue 65, and to the phosphates of the incoming TFV-DP, it does not appear to interact directly with these structural elements.

Discussion

We have discovered a novel HIV mutation that causes high-level resistance to TFV-DF. We have also determined the biochemical mechanism of this resistance. TFV-DF is a valuable NRTI therapeutic option for patients infected with multi-drug resistant Q151Mc HIV-1 [22]. We demonstrate here that Q151Mc can acquire an additional mutation, K70Q, which expands the multi-drug resistance to include high-level resistance to TFV-DF. We identified this mutant during genotypic analysis of clinical isolates from an HIV-infected patient who was not responding to TFV-DF. The K70Q/Q151Mc set of mutations is currently rare among HIV-infected patients. However, we believe that similar to K65R, its prevalence will increase, as tenofovir use continues to rise. Our virological studies with recombinant viruses confirmed that the observed enhancement and expansion of multi-drug resistance is the consequence of the addition of K70Q to Q151Mc HIV. Recently, the concept of clinical cut-offs (CCOs) has been introduced to improve the prediction of drug resistance during antiretroviral therapies. CCOs are better correlated with virologic response than biological cut-offs [51,52]. Importantly, K70Q/Q151Mc is 10 times less susceptible to TFV-DF than WT HIV-1, whereas the CCOs for TFV-DF is defined as a 2.1-fold reduction in virologic response to this inhibitor. Moreover, K70Q/Q151Mc is at least twice as resistant to TFV as the well-known TFV-resistant K65R in the background of Q151Mc (as reported in the Stanford HIV Drug Resistance Database).

Previous studies have offered insights into the drug resistance mechanism of similar mutations (K70E, K70G, K70R, and K70T). Specifically, K70E was selected in patients with virological failure after TFV-DF-based antiviral therapy [53,54,55]. K70T emerged in the background of Q151Mc during *in vitro* selection by TFV-DF [56]. K70R is a key mutation involved in resistance to AZT and appears in the background of other excision enhancement mutations [2,3,57]. In our case, a new mutation (K70Q) was

Table 2. Pre-steady state kinetic constants for binding and incorporation of dATP and TFV-DP by WT, K70Q, Q151Mc and K70Q/Q151Mc HIV-1 RT.

Pre-steady state kinetic constants[a]

Enzyme[b]	dATP			TFV-DP			Selectivity[c]	Resistance[d]
	k_{pol} (s^{-1})	K_d (μM)	k_{pol}/K_d ($\mu M^{-1}\cdot s^{-1}$)	k_{pol} (s^{-1})	K_d (μM)	k_{pol}/K_d ($\mu M^{-1}\cdot s^{-1}$)		
WT	6.3±0.5	2.6±0.1	2.4±0.2	2.8±0.08	1.9±0.2	1.47±0.07	1.6	-
K70Q	8.4±0.4	3.8±0.6	2.2±0.4	3.1±0.4	8.6±1.5	0.36±0.08	6.1	3.8
Q151Mc	17.9±0.4	5.4±0.5	3.3±0.3	1.3±0.03	4.3±0.8	0.3±0.06	11	6.9
K70Q/Q151Mc	14.6±1.6	5.0±0.07	2.9±0.3	1.0±0.03	8.9±2.1	0.11±0.03	26.3	16.4

[a]Data are means ± standard deviations from at least three independent experiments.
[b]The sequence of HIV RT WT and mutant derived from BH10.
[c]Selectivity is defined as $(k_{pol}/K_d)_{dATP}/(k_{pol}/K_d)_{TFV\text{-}DP}$.
[d]Resistance (fold) is calculated as $selectivity_{mutant}/selectivity_{WT}$.
doi:10.1371/journal.pone.0016242.t002

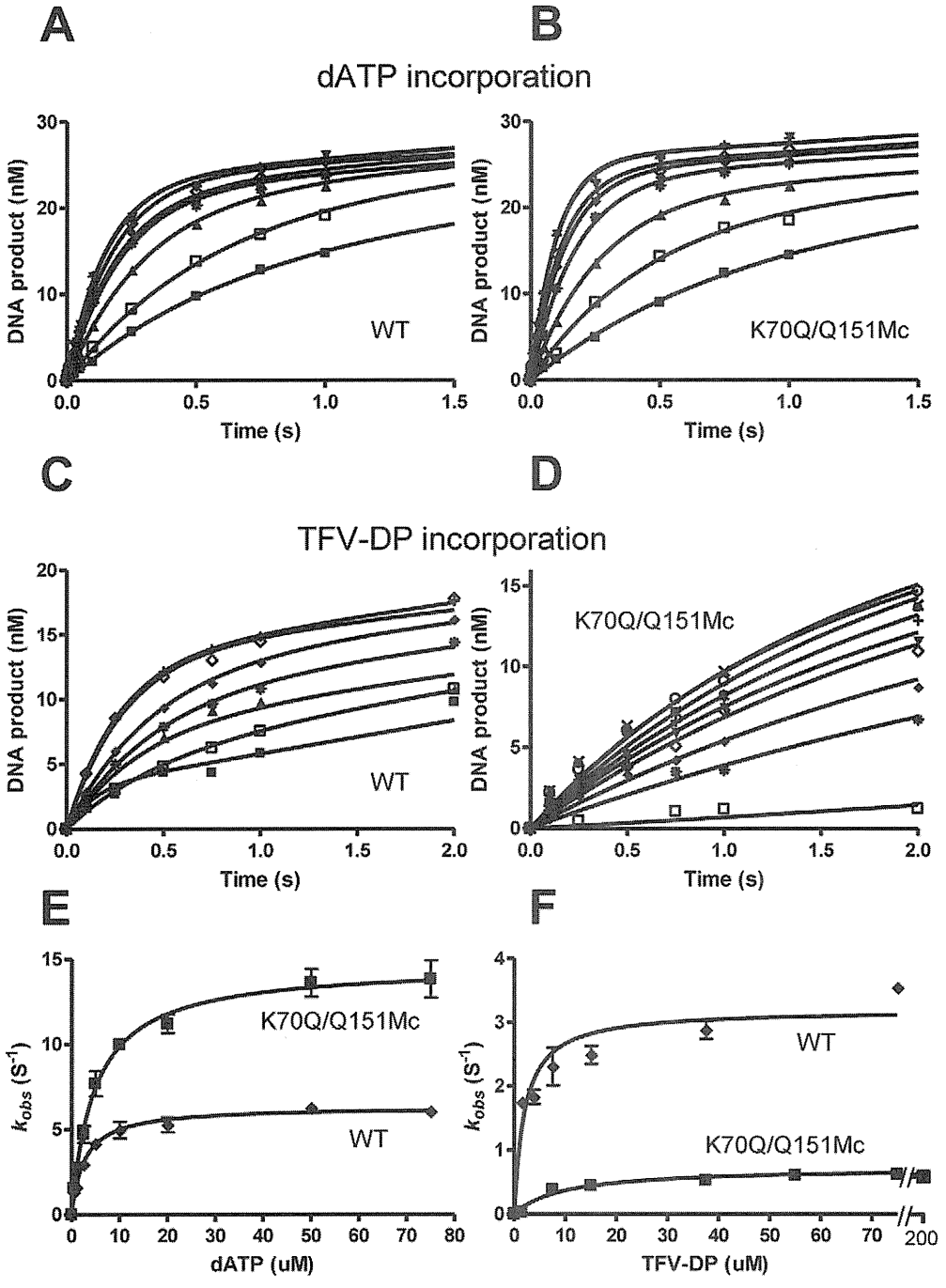

Figure 4. Pre-steady state kinetics of incorporation of dATP or TFV-DP by WT and K70Q/Q151Mc HIV-1 RTs. Single-nucleotide incorporation of dATP (panels A, B, and E) or TFV-DP (panels C, D, and F) by WT (panels A, C, E, and F) and K70Q/Q151Mc (panels B, D, E, and F). Formation of extended primer products in the reactions with WT RT and K70Q/Q151Mc RT were measured at 5 ms to 5 s time points, using the following dATP concentrations: 0.5 (■), 1 (□), 2.5 (▲), 5 (*), 10 (♦), 20 (◇), 50 (▼) and 75 μM (+). Incorporation of TFV was measured at 0.1–10 s reactions and at the following TFV-DP concentrations: 0.75 (■), 1.5 (□), 3.75 (▲), 7.5 (*), 15 (♦), 37.5 (◇) and 75 μM (+) for reactions with WT RT (panel C), and 1.5 (□), 7.5 (*), 15 (♦), 37.5 (◇), 55 (▼), 75 (+), 112.5 (•), 150 (○) and 200 μM (x) for reactions with K70Q/Q151Mc RT (panel D). (E) The amplitudes of the burst phases from the dATP reactions shown in panels A (WT, [♦]) and B (K70Q/Q151Mc, [■]) were plotted as a function of dATP concentrations. (F) The amplitudes of the burst phases from the TFV-DP reactions shown in panels C (WT, [♦]) and D (K70Q/Q151Mc, [■]) were plotted as a function of TFV-DP concentrations. The solid lines in panels A, B, C, and D represent the best fit of data to the burst equation. Each point represents the average values of three experiments.
doi:10.1371/journal.pone.0016242.g004

identified in a patient infected with Q151Mc HIV-1 during the course of TFV-DF-based antiviral therapy. The International AIDS Society-USA publishes [58] every year a list of HIV-1 drug resistance mutations compiled by a panel of experts charged with the goal of delivering accurate, unbiased, and evidence-based information for use by HIV clinical practitioners. In order for a novel mutation to be accepted in the list it should meet at least *one* of the following criteria: 1) *in vitro* passage experiments or

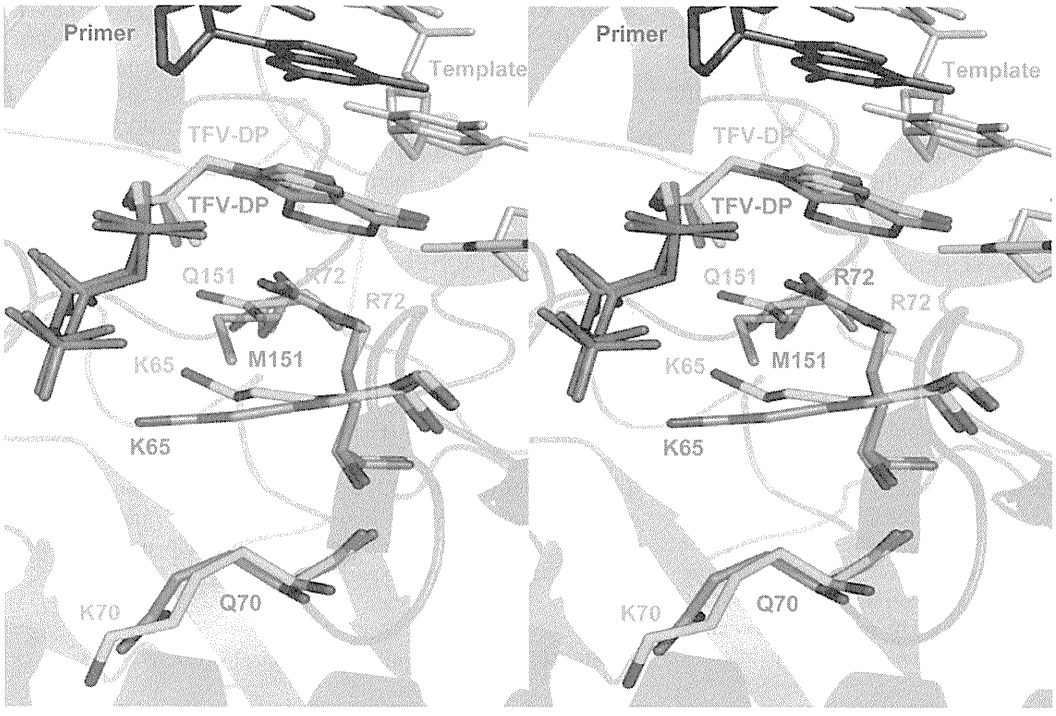

Figure 5. Stereo view of TFV-DP in the polymerase active site of WT RT and K70Q/Q151Mc RT. WT RT residues are shown as cyan sticks, K70Q/Q151Mc RT residues are shown as purple sticks. The primer strand is shown as dark gray sticks, template strand as light gray sticks. The fingers and palm subdomains are shown as blue and red cartoons, respectively.
doi:10.1371/journal.pone.0016242.g005

validation of contribution to resistance by using site-directed mutagenesis; 2) susceptibility testing of laboratory or clinical isolates; 3) nucleotide sequencing of viruses from patients in whom the drug is failing; 4) correlation studies between genotype at baseline and virologic response in patients exposed to a drug. Our study has unambiguously demonstrated that K70Q meets at least the first three criteria: evidence for criterion #1 is shown in Figure 2; for criterion #2 in Figures 1 and 2; and for criterion #3 in Figure 1 and Figure S1. Therefore, the K70Q mutation meets the criteria of a clinically relevant mutation.

In addition to the clinical and virological studies, we used biochemical techniques to determine the mechanism of TFV resistance imparted by the K70Q mutation to Q151Mc RTs. We used primer extension assays to show that K70Q/Q151Mc RT is less susceptible to TFV-DP than WT and Q151Mc RTs. We demonstrated that the mechanism of this resistance is not based on excision. On the contrary, we showed that the ATP-based excision of the mutant enzymes was slightly decreased with respect to WT RT, possibly because of decreased affinity of the mutant enzymes for the ATP excision substrate, incurred by changes in the binding environment of ATP, such as the loss of lysine at position 70.

Using transient-state kinetics we unambiguously established that the overall mechanism of K70Q/Q151Mc resistance to TFV is due to enhanced discrimination between the natural dATP substrate and TFV-DP. While all mutant enzymes had comparable efficiency of dATP incorporation, they displayed varying affinity and turnover rates of incorporation. It appears that the stronger effect of the enhanced discrimination overcomes the slight increase in sensitivity due to the small increase in excision. As a result, the mutant enzymes are resistant to the inhibitor.

Mutations at position 70 of RT have been known to confer NRTI resistance by two distinct mechanisms: K70R combined with at least two excision enhancing mutations, D67N and T215Y, enhances ATP-mediated excision of AZT and d4T [1,2,3,48] (*excision–dependent mechanism*). On the other hand, K70E causes resistance to 3TC, TFV, and ABC by lowering the maximum rate of inhibitor incorporation by RT (k_{pol}*-dependent exclusion mechanism*) [55]. Our results establish that in the background of Q151Mc, K70Q causes TFV resistance through a third mechanism: by decreasing the binding affinity of the inhibitor (K_d*-dependent exclusion mechanism*). Taken together, these findings highlight the remarkable ability of RT to use separate mutations at a single position to acquire NRTI resistance through three different mechanisms.

Our cell-based assays with infectious HIV-1 show that Q151Mc remains susceptible to TFV-DF, a finding consistent with previous reports [22]. Similarly, clinical isolates deposited at the Stanford HIV resistance database and carrying the Q151Mc mutation were also susceptible to TFV-DF, unless they also had the K65R mutation. However, pre-steady state characterization of TFV-DP incorporation by Q151Mc in this work (Table 2) and by others [59] showed that Q151Mc is less susceptible to TFV-DP than WT RT. This small discrepancy may be the result of potential differences in DNA-dependent and RNA-dependent DNA synthesis, or the result of the slightly increased excision of Q151Mc RT compared to WT RT (Fig. 3B and C).

To gain insights into the possible structural changes caused by the addition of K70Q to Q151Mc, we compared the molecular model of K70Q/Q151Mc RT/DNA/TFV-DP with the crystal structure of WT RT/DNA/TFV-DP [45] (Fig. 5). The network of hydrogen bonds involving the side-chains of K65, R72, and Q151 in the WT structure [26,27,54], is disrupted in the mutant structure. Also, Q151M and associated mutations A62V, V75I, and F77L are likely to modify the hydrophobic core of the fingers. We and others have previously shown that the side-chains of residues 72 and 65 interact with each other [35] and with Q151

and the α- and γ-phosphates of the incoming dNTP [26] or TFV-DP [45]. The functions of these residues have been established by several biochemical studies [21,25,60,61,62,63]. The reduction in polymerase rate (k_{pol}) and in binding affinity for TFV-DP (increased $K_{d.TFV\text{-}DP}$) may be the consequence of one or more such structural changes. Our molecular dynamics simulation experiments suggested a re-arrangement in the position of the side chain of K65, which is a catalytically important residue. While the precise effect of this change is not clear at this point, such changes could influence the overall binding of the substrate and/or the rate of nucleotide incorporation. Moreover, such movement of K65 in the presence of a mutation at position 70 is consistent with our previously reported crystallographic data, which established that there is an interplay between the positioning of the side chains at positions 70 and 65 [64]. Ongoing crystallographic studies are expected to provide more detailed structural insights into the role of K70Q in drug resistance.

In summary, we report here clinical data showing that addition of the K70Q mutation to the Q151Mc background confers high-level HIV resistance to TFV-DF and enhances resistance to other NRTIs. The biochemical mechanism of the TFV resistance is based on reduced binding affinity and incorporation of TFV-DP. Detection of this novel pattern of TFV-DF resistance may help adjust therapeutic regimens for the treatment of patients infected with multi-drug resistant HIV-1.

Supporting Information

Figure S1 Amino acid sequence alignment of the RT regions (amino acid 32 to 560) of the clinical isolates at time points 1 to 2 (see Figure 1A).
(DOC)

Figure S2 Effects of RT mutations K70Q, Q151Mc, or K70Q/Q151Mc on DNA primer extension activity and on ATP-based excision activities. (A) Effect of varying concentrations of TFV-DP on the primer extension activities of HIV-1 WT and mutant RTs. The experiments were carried out in the presence and absence of 3.5 mM ATP (marked as ATP (+) and ATP (−), respectively). Addition of ATP in the polymerization mixture allows measurement of the net sum of DNA polymerization and ATP-based excision activities. (B) Time dependence of ATP-based rescue of TFV-terminated primers. (C) ATP-based rescue was dependent on concentration of ATP.
(PPTX)

Figure S3 Pre-steady state incorporation of dATP or TFV-DP by K70Q and Q151Mc HIV-1 RTs. Single-nucleotide incorporation of dATP (panels A, B, and E) or TFV-DP (panels C, D, and F) by K70Q (panels A, C, E, and F) and Q151Mc (panels B, D, E, and F). Formation of extended primer products in the reactions with K70Q RT and Q151Mc RT were measured at 5 ms to 5 s time points, using the following dATP concentrations: 0.5 (■), 1 (□), 2.5 (▲), 5 (*), 10 (♦), 20 (◇), 50 (▼) and 75 μM (+). Incorporation of TFV was measured at 0.1–10 s reactions and at the following TFV-DP concentrations: 0.75 (■), 1.5 (□), 3.75 (▲), 7.5 (*), 15 (♦), 37.5 (◇) and 75 μM (▼) for reactions with K70Q RT (panel C), and 3.75 (▲), 7.5 (*), 37.5 (◇), 55 (▼), 75 (+) and 112.5 (•) for reactions with Q151Mc RT (panel D). (E) The amplitudes of the burst phases from the dATP reactions shown in panels A (K70Q, [▲]) and B (Q151Mc, [▼]) were plotted as a function of dATP concentrations. (F) The amplitudes of the burst phases from the TFV-DP reactions shown in panels C (K70Q, [▲]) and D (Q151Mc, [▼]) were plotted as a function of TFV-DP concentrations. The solid lines in panels A, B, C, and D represent the best fit of data to a burst equation. Each point represents average values of three experiments.
(PPTX)

Table S1 Drug susceptibility of clinical isolates.
(DOC)

Table S2 Drug susceptibility of HIV-1 variants carrying mutation at residue 70.
(DOC)

Table S3 Drug susceptibility of HIV-1 variants carrying mutation at residue 70 in the background of Q151M complex.
(DOC)

Acknowledgments

We thank Yukiko Takahashi and Fujie Negishi for sample preparation, and Dr. Hiroyuki Gatanaga and Dr. Michael A. Parniak for helpful discussions.

Author Contributions

Conceived and designed the experiments: AH ENK SO SGS. Performed the experiments: AH MMS KAK EM YS KS. Analyzed the data: AH MMS KAK KS SGS. Contributed reagents/materials/analysis tools: AH ENK SGS OS. Wrote the paper: AH ENK KS SGS.

References

1. Meyer PR, Matsuura SE, Mian AM, So AG, Scott WA (1999) A mechanism of AZT resistance: an increase in nucleotide-dependent primer unblocking by mutant HIV-1 reverse transcriptase. Mol Cell 4: 35–43.
2. Boyer PL, Sarafianos SG, Arnold E, Hughes SH (2001) Selective excision of AZTMP by drug-resistant human immunodeficiency virus reverse transcriptase. J Virol 75: 4832–4842.
3. Arion D, Kaushik N, McCormick S, Borkow G, Parniak MA (1998) Phenotypic mechanism of HIV-1 resistance to 3′-azido-3′-deoxythymidine (AZT): increased polymerization processivity and enhanced sensitivity to pyrophosphate of the mutant viral reverse transcriptase. Biochemistry 37: 15908–15917.
4. Singh K, Marchand B, Kirby KA, Michailidis E, Sarafianos SG (2010) Structural aspects of drug resistance and inhibition of HIV-1 reverse transcriptase. Viruses 2: 606–638.
5. Mas A, Parera M, Briones C, Soriano V, Martinez MA, et al. (2000) Role of a dipeptide insertion between codons 69 and 70 of HIV-1 reverse transcriptase in the mechanism of AZT resistance. EMBO J 19: 5752–5761.
6. Matamoros T, Franco S, Vazquez-Alvarez BM, Mas A, Martinez MA, et al. (2004) Molecular determinants of multi-nucleoside analogue resistance in HIV-1 reverse transcriptases containing a dipeptide insertion in the fingers subdomain: effect of mutations D67N and T215Y on removal of thymidine nucleotide analogues from blocked DNA primers. J Biol Chem 279: 24569–24577.
7. Meyer PR, Lennerstrand J, Matsuura SE, Larder BA, Scott WA (2003) Effects of dipeptide insertions between codons 69 and 70 of human immunodeficiency virus type 1 reverse transcriptase on primer unblocking, deoxynucleoside triphosphate inhibition, and DNA chain elongation. J Virol 77: 3871–3877.
8. Kew Y, Olsen LR, Japour AJ, Prasad VR (1998) Insertions into the beta3-beta4 hairpin loop of HIV-1 reverse transcriptase reveal a role for fingers subdomain in processive polymerization. J Biol Chem 273: 7529–7537.
9. Boyer PL, Sarafianos SG, Arnold E, Hughes SH (2002) Nucleoside analog resistance caused by insertions in the fingers of human immunodeficiency virus type 1 reverse transcriptase involves ATP-mediated excision. J Virol 76: 9143–9151.
10. Menendez-Arias L (2008) Mechanisms of resistance to nucleoside analogue inhibitors of HIV-1 reverse transcriptase. Virus Res 134: 124–146.
11. Sarafianos SG, Marchand B, Das K, Himmel DM, Parniak MA, et al. (2009) Structure and function of HIV-1 reverse transcriptase: molecular mechanisms of polymerization and inhibition. J Mol Biol 385: 693–713.
12. Sarafianos SG, Das K, Clark AD, Jr., Ding J, Boyer PL, et al. (1999) Lamivudine (3TC) resistance in HIV-1 reverse transcriptase involves steric hindrance with beta-branched amino acids. Proc Natl Acad Sci U S A 96: 10027–10032.
13. Gao HQ, Boyer PL, Sarafianos SG, Arnold E, Hughes SH (2000) The role of steric hindrance in 3TC resistance of human immunodeficiency virus type-1 reverse transcriptase. J Mol Biol 300: 403–418.